Politecnico di Torino

ETH zürich

Master's Degree in Biomedical Engineering

Monitoring in-vitro neural dynamics using high-density microelectrode arrays

Supervisors:

Prof. Chiara TONDA-TURO
Prof. Andreas HIERLEMANN

Candidate:

Alessandro FORASTIERE

Advisors:

Dr. Fernando CARDES GARCIA
Dr. Hasan ULUSAN

Academic Year 2021/2022

October 2022

Abstract

Synaptic plasticity is thought to be the main process underlining how we learn, store memories, and even recover from injuries. With this term, we refer to the ability of the brain to change the strength of its synaptic connections in response to stimuli: an increase in the synaptic transmission is called potentiation, while a decrease results in what is named depression. One particular form of synaptic plasticity, called spike-timing dependent plasticity (STDP), emphasizes the temporal order and time interval between the presynaptic and postsynaptic potentials. In order to study the complex phenomena entailing neural plasticity, intracellular techniques for recording and stimulation have been extensively used. Although very powerful, they do not allow us to measure the electrical activity in a population of neurons; in addition, their invasive nature severely limits cell viability up to a few hours. To face these drawbacks, extracellular recording methods started to arise, since they enable non-invasively and simultaneously recording of neural activity from different sites. Thanks to the advancements in microtechnology, it is now possible to design high-density microelectrode arrays (HD-MEA), employing the complementary metal oxide semiconductor (CMOS) technology. Here, a newly developed CMOS HD-MEA was used with the goal of providing a new tool to study STDP. The HD-MEA features 59 760 microelectrodes, which is the largest number to date, arranged in a 4.48 x 2.43 mm^2 sensing area with an inter-electrodic distance of 13.5 μm. The device was exploited to monitor the activity of rat cortical cell cultures in vitro, by recording the signal from the electrodes after having received Pt-black electrodeposition for noise reduction. The spike sorter Tridesclous was chosen to detect neurons on the chip and cross-correlogram analysis was performed to find pairs of potentially connected neurons. Nevertheless, cell viability and hardware issues did not allow us to assess STDP through stimulation. For these reasons, the results from spontaneous electrophysiological recording and stimulation in saline solution show the limits of the device and the necessity of a new culturing protocol to be developed, with the aim of exploiting all the potentiality this HD-MEA can offer to neuroscientists.

Table of contents

List of tables

List of figures

Acronyms and abbreviations

Abbreviation	Definition
ACG	Auto-correlogram
AIS	Axon initial segment
$AMPA_R$	α-amino-3-hydroxy-5-methyl-4-isoxazole propionic acid receptor
AP	Action potential
AP-2	Clathrin adaptor complex
Ca^{2+}	Calcium ion
CaMKII	Calmodulin-dependent protein kinase II
CCG	Cross-correlogram
CMOS	Complementary-metal-oxide semiconductor
CNS	Central Nervous System
DAC	Digital-to-analog converter
DIV	Days in vitro
EAP	Extracellular action potential
EPSP	Excitatory postsynaptic potential
FPGA	Field-programmable gate array
GABA	γ-Aminobutyric acid
GUI	Graphical User Interface
HD-MEA	High-density microelectrode array
IAP	Intracellular action potential
IPSP	Inhibitory postsynaptic potential
K^+	Potassium ion
LFP	Local field potential
LTD	Long-term depression

LTP	Long-term potentiation
MAD	Median absolute deviation
MEA	Microelectrode array
Mg^{2+}	Magnesium ion
Na^{+}	Sodium ion
$NMDA_R$	N-methyl-D-aspartate receptor
PBS	Phosphate Buffer Saline
PEI	Poly(ethyleneimine)
PP1	Protein phosphatase 1
PSD	Power spectral density
PSP	Postsynaptic potential
Pt-black	Platinum-black
SNARE	soluble N-ethylmaleimide-sensitive factor attachment protein receptor
SNR	Signal-to-noise ratio
STDP	Spike-timing-dependent plasticity

Introduction

The brain is arguably the most fascinating organ in the human body. It contains around 100 billion neurons forming highly complex networks capable to perform lots of amazing tasks, like motor movement, thinking, managing emotions, and memory to name a few. During the last years, neuroscience has been growing by leaps and bounds, motivated by the necessity to effectively treat the majority of neurodegenerative diseases and disorders. In parallel, an enormous push to neuroscience research has been given by the strong desire to understand the inner workings entailing how the brain processes the information coming from the external physical and emotional experiences, and especially the expression of how it can store new memories and decide to discard the past ones. Explaining the physics behind these abstract events within the brain is a challenge that still has no answer but, according to many neuroscientists, synaptic plasticity is the main mechanism by which our brain operates to process the stimuli received. Synaptic plasticity is a term that is used to describe how the synapses change in response to use or disuse; they can undergo potentiation (or strengthening) if repeatedly used or depression (weakening) if not. There is one particular form of synaptic plasticity, which is called spike-timing dependent plasticity (STDP) which emphasizes the role of the relative timing between the presynaptic and postsynaptic action potentials: potentiation will take place when presynaptic action potential leads to the postsynaptic action potential with a time delay within 0 – 20 ms, while postsynaptic leading presynaptic activity within 0 – 100 ms promotes depression.

Studying the intricate behavior of neuronal cells requires high spatiotemporal-resolution techniques able to provide the simultaneous measurement of many parameters. Intracellular methods are very accurate but they need to access the cell interior with the electrodes, limiting the cell viability time up to a few hours because of their invasive nature. These issues, along with the impossibility to investigate a large number of cells at the same time, represent a huge limitation in the study of neuronal phenomena. On the contrary, extracellular recordings represent a non-invasive alternative to the aforementioned method, enabling long-term measurements of multiple cells employing a large number of

microelectrodes arranged in a tiny sensing area. Complementary-metal-oxide-semiconductor microelectrode arrays (CMOS-MEAs) are one of the most promising tools which can be exploited to perform electrophysiological investigations in large populations of electrically active cells down to the sub-cellular resolution. CMOS technology allows the design of high-density microelectrode arrays (HD-MEAs), where thousands of microelectrodes are closely spaced in a small area of a few mm^2. In this thesis, a CMOS-based HD-MEA consisting of 59 760 microelectrodes was employed as a potential tool in the study of STDP. The CMOS chip possesses a sensing area of 4.48 x 2.43 mm^2 with an inter-electrode distance of 13.5 μm and provides electrophysiology measurement functions as well as stimulation capability. The goal was to select pairs of connected neurons and stimulate them with a predefined time delay to induce synaptic plasticity and discover when and in which measure potentiation and depression will occur. The neuronal cultures were monitored over time after sorting all of the spikes from the recorded signals, by the means of a specific spike sorting algorithm. This allowed us to associate each spike to its respective neuron; once the spike trains were stored, cross-correlograms were analyzed to find potentially connected neurons that can be exploited to perform pair stimulation. According to various studies, the most sensitive region to stimulation is the axon initial segment (AIS) compartment, therefore the electrodes chosen for applying the stimuli are the ones situated beneath the AIS, where the highest potential is recorded. Afterward, successive steps have been planned but not carried out throughout the project, due to various issues regarding the cell cultures and the setup. First, monophasic and biphasic stimulation waveforms with different amplitudes were designed to be tested which one was able to most effectively evoke the action potential of the single neuron. Next, pair stimulation would have been applied, by varying the time delay between the two stimuli. Finally, the synaptic changes would have been again evaluated using cross-correlograms to estimate the effect of the stimulation.

1 Background

This chapter gives a general, unpretentious, but also a comprehensive overview of neurophysiology to better understand the topics of synaptic plasticity, spike-timing-dependent plasticity, and Hebbian rules which will be described later in the next sections. The most important element which is the common thread of this thesis is the neuron. The neuron, or nerve cell, is the basic functional unit of the human nervous system, allowing us to perceive sensations, form new memories, learn, and much more. The neuron is an electrically excitable cell specialized in transferring information via electrochemical signals both over short and long distances with no attenuation.

1.1 Neuron structure

The main feature of a nerve cell is the presence of extensions (Figure 1.1a), which are fundamental for communication between neurons: these projections are also called neurites and can be divided into dendrites or axons, depending on whether they are responsible for receiving or sending signals respectively. All neurons have a cell body, or soma, from which neurites originate, representing the cell control center and containing the nucleus as well as the necessary organelles for cell functions. The dimensions of the cell body are relatively small compared to the whole cell volume since it generally occupies one-tenth of the total [1].

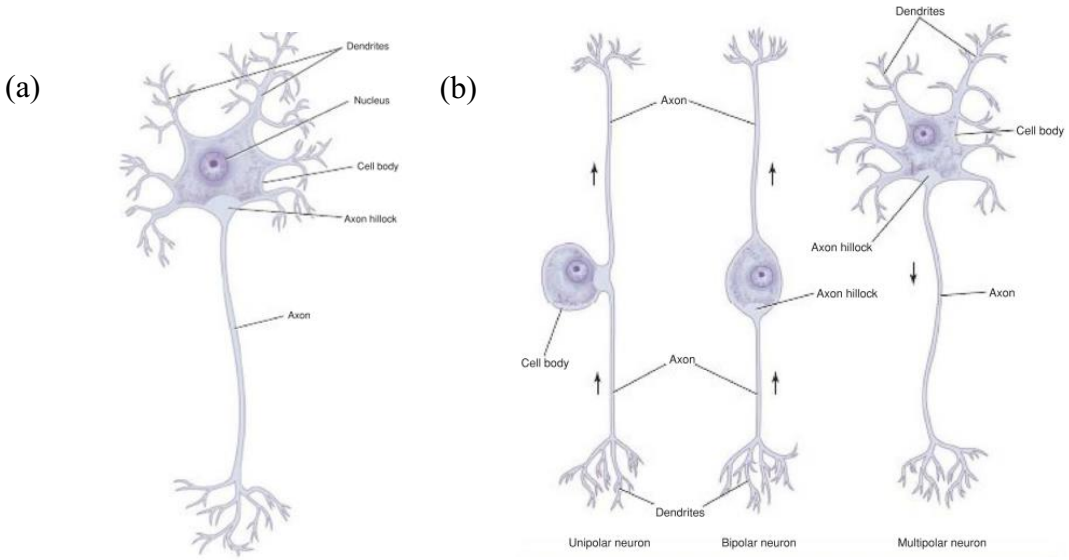

Figure 1.1 Neuron structure. (a) Schematic representation of a neuron. (b) Types of neurons according to morphology [2].

Neurons can be classified in multiple ways, like size or function, but generally, the most recurrent classification is based on the morphology of the neurites which emanate from the soma [2]; according to this classification we distinguish (Figure 1.1b):

- multipolar cells, formed by a lot of dendrites and a single long axon. They represent the main cell type in the brain and spinal cord;
- bipolar cells, which have one dendrite and one axon extending from each end of the cell body. These neurons are specialized in sensory transmission; we can find them in the retina, sensory cochlea, and vestibular ganglia;
- unipolar cells, possessing a single projection which in turn divides into two different branches, one enters the central nervous system (CNS) and the other one enters the peripheral nervous system. They can be found in the dorsal root ganglion.

The organelles in a nerve cell are common to any other cell type in the human body, whereas the most interesting structures of a neuron are its neurites which make this cell not only structurally but also functionally unique.

Dendrites are ramified extensions capable of receiving electrochemical stimuli from nearby cells and transferring the corresponding information toward the soma. They typically resemble a tree-like arborization and have a cytoplasm similar to that of the cell body; especially, they contain a high number of ribosomes, which means they have a high degree

of protein synthesis to support signal transmission [3]. On the other hand, axons take the signals coming from the cell body and transfer them to the target cell. Another difference is that axon is relatively longer than dendrites, the majority of them are some millimeters long in the human CNS, but they can reach one meter or more when considering motor neurons; dendrites, instead, have a length in the order of micrometers. There is also variability in axon diameter, with the key aspect that a longer diameter enables very fast transmission while a shorter diameter slower conduction.

1.2 Action potential

To understand how neurons communicate with each other, it is worth describing what an action potential is since it is the element responsible for the flow of electrical signals within a neuron. In the resting or unstimulated state, the inside of a nerve cell is negative relative to the extracellular environment; if we place an electrode into the cell body and a reference electrode into the extracellular matrix, we can observe a membrane potential of approximately -70 mV, with a slight variability depending on the neuron being examined [4]. This potential takes into account all the ion concentration gradients as the main ions responsible for the resting membrane potential are sodium Na^+ and potassium K^+: Na^+ has a greater concentration outside the cell compared with the interior and it is pumped out by the Na^+/K^+-ATPase active transporter; while K^+ has higher concentration into the cell compared to the outside. Since the membrane potential depends on the membrane permeability to each ion and K^+ permeability is higher than Na^+ at the resting state, the resting membrane potential is closer to the K^+ equilibrium potential (-90 mV). Active ion pumps establish the driving force for the generation of electrical signals and their presence is balanced by that of the ion channel transporters, which passively permit the diffusion of the ions down their concentration gradient, based on the permeability of the channel to its specific ion.

1.2.1 Action potential: generation

When the membrane becomes more permeable to Na^+ (because of the opening of Na^+ ion channels), and this normally happens when the cell receives a stimulus, the

membrane potential becomes more positive (depolarization) since an inward positive current of Na^+ ions occurs (Figure 1.2). If a threshold potential of approximately -55 mV is overcome, an upstroke is observed thanks to the opening of voltage-gated sodium channels, which generate a strong increase of the potential, reaching a positive value around +30 mV [1]. When Na^+ ion channels start to close, voltage-gated potassium channels open since they are less sensitive to the potential and consequently require a higher level of depolarization to be opened. At the time of the voltage peak (overshoot), Na^+ ion channels close, and an absolute refractory period (1 ms) in which they cannot be open again begins, this is to distinguish it from the relative refractory period (2 ms) during which a sufficiently stronger stimulus can excite the cell. K^+ is the only ion most capable of flowing through the cell at this time, leading to a decrease in the potential up to -90 mV (hyperpolarization). After that, K^+ ion channels close and the original equilibrium is restored by the Na^+/K^+ ion pump. The process described is called action potential (AP), or spike, and it is very fast, typically the whole process lasts thousandths of a second and starts at the level of the axon initial segment (AIS), a micro-domain at the base of the axon [5]. Another feature is that an AP follows the all-or-none rule [6], meaning that neither a weak nor strong action potential exists, but it always has the same entity once it has been triggered. Neurons can modulate the frequency of their AP to code the power of a stimulus: if the amplitude of the triggering stimulus increases, the frequency increases as well, and vice versa.

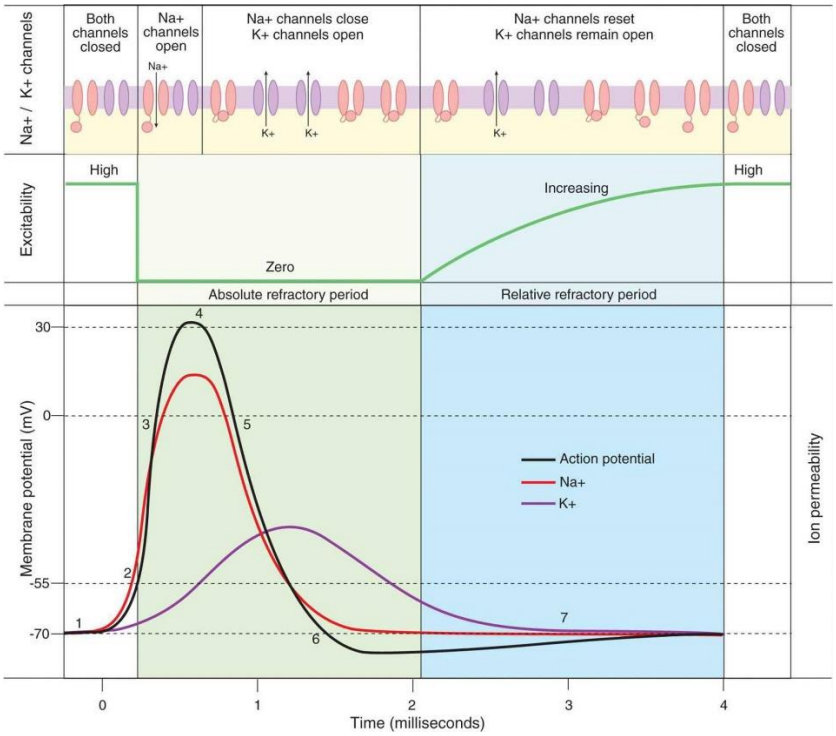

Figure 1.2 Changes in the Na^+ and K^+ ion channels, excitability, membrane potential, and relative ion permeability during an action potential. The numbers along the membrane potential curve indicate: 1) resting, 2) threshold voltage overcome and opening of the voltage-gated Na^+ channels, 3) fast Na^+ flow according to the electrochemical gradient, 4) Na^+ ion channels close, 5) K^+ ion channels conductance increases, 6) hyperpolarization and 7) return to the resting state [7].

1.2.2 Action potential: propagation

An AP forms at the AIS in response to either mechanical stress or commonly chemical stimuli and it propagates towards the axon terminal (retrograde propagation), with no possibility to go back (anterograde propagation) since this is prevented in and by the refractory period state described before, which the region of the axon undergoes just after have been depolarized. The propagation of an AP can be easily understood as the movement of positive charges (Figure 1.3): when the AP in one region is triggered, the intracellular compartment presents a positive charge, while the adjacent region has a negative charge compared to the extracellular environment; consequently, positive charge is attracted toward the negative adjacent region and this allows a new AP to form if the depolarization is sufficient. This spreading process will repeat along the axon until the terminal area is reached, and since Na^+ continues to flow in every depolarizing area, the signal is not attenuated.

Many axons of the human neurons are covered with a stratified insulating substance produced by the glial cells (cell which assist brain development), called myelin, which features a very high electric resistance preventing current dispersion. Segments of myelin alternate with little uncovered membrane sections, the Ranvier nodes; voltage-gated ion channels are only expressed in the inter-nodal regions and the conduction, also known as saltatory conduction, "jumps" from one node to another and results faster than non-myelinated axons.

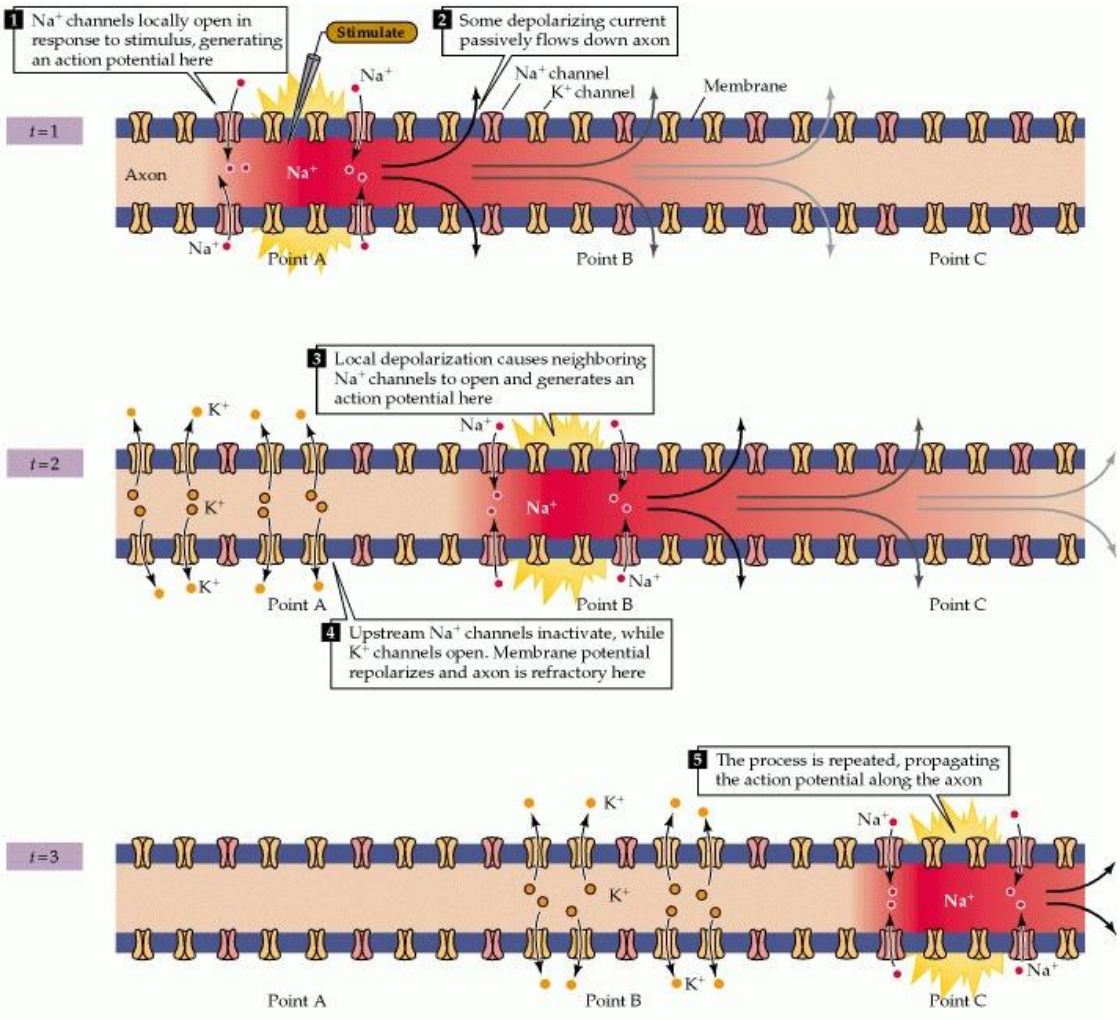

Figure 1.3 Action potential conduction along the axon [8].

1.3 The synapse

The most essential part of the signal transmission between two neurons is called the synapse. A synapse is a region where two neurons, or a neuron and a muscle cell, form a functional connection. The signal-passing cell is called presynaptic neuron while the target nerve cell postsynaptic neuron: the most common form of the synapse is that we can observe between the axon of the presynaptic cell and the dendrite of the postsynaptic one (Figure 1.4a**)**. The majority of the neurons can make synapses with 1,000 or more other neurons and receive up to 10,000 connections from other neurons [2]. Synapses are divided into chemical and electrical synapses, with the former representing the type most diffused in the human brain.

Electrical synapse allows for very rapid conduction, in the fraction of milliseconds, with a probability of transmission of almost 100% [8]. The membranes of both the cells are close, and communication is possible thanks to the presence of connexons, proteins that create pores (or gap junctions) within the cell and its adjacent one, permitting the flow of ions through them. Electrical synapses are quite rare in the human species but they have been found in some regions of the brain, e.g., the neocortex, hippocampus, and thalamus [9].

The chemical synapse represents the most common type of synapse in the human body, and it involves the action of a chemical substance, or neurotransmitter, which is released in the synaptic cleft by the presynaptic neuron in response to the AP, then it diffuses towards the postsynaptic cell membrane where it binds to specific receptors. The synaptic cleft is typically 0.02 μm wide in CNS and 0.05 μm at the neuromuscular junction [10]; these tiny dimensions allow the neurotransmitter to soon pile up and reach high concentration levels in a very short time. The neurotransmitter is contained in a certain number of vesicles densely clustered in an area of the presynaptic neuron known as active zone (Figure 1.4a and 1.4b), it is then expelled via exocytosis and is cleared out from the synaptic cleft by enzymatic degradation or recycled from the presynaptic cell or other neuroglia cells to stop the neurotransmitter activity.

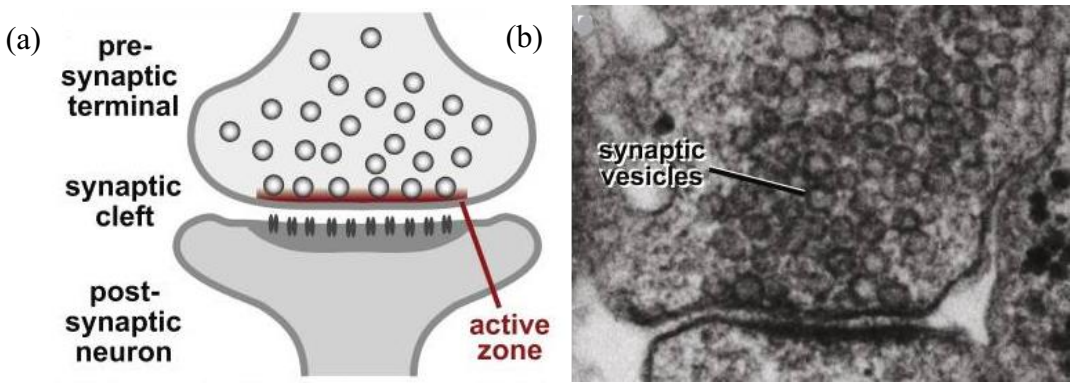

Figure 1.4 Synapse and active zone representations. (a) Schematic drawing of a chemical synapse between the axon terminal of a presynaptic neuron and the dendrite of a postsynaptic cell. The active zone, represented in red, is where synaptic vesicles are clustered before the release of neurotransmitter. (b) Electron micrograph of the active zone in a hippocampal neuron [11].

1.3.1 Neurotransmitter release

Transmission via chemical signals allows for a highly versatile tuning of coding information than electrical transmission since neurotransmitters can evoke either short or long-lasting responses, this is also the reason why chemical synapses represent the most abundant type in the nervous system.

Many hypotheses have been developed to describe signaling mechanisms through chemical synapses, the most known is the so-called "Calcium hypothesis" (Figure 1.5). When an AP arrives at the presynaptic terminal, it causes the opening of the voltage-gated calcium channels, Ca^{2+} then associates with a protein docked to the vesicles called synaptotagmin, which senses Ca^{2+} and catalyzes the fusion of neurotransmitter-containing vesicles with the membrane [12]. The fusion of the vesicles with the presynaptic membrane is mediated by a set of proteins forming the so-called *soluble N-ethylmaleimide-sensitive factor attachment* protein *receptor* (SNARE) complex, which facilitates the formation of a fusion pore by inducing distortion in the membrane and leading to the release of the neurotransmitter [13]. Another protein called complexin plays an important role in this process because it prevents a constitutive release of synaptic vesicles opposing the formation of the SNAREs complexes [14]. After the release of the neurotransmitter, vesicles are recycled by endocytosis via the clathrin-dependent mechanism which prepares for new rounds of synaptic transmission. This process involves the clathrin adaptor complex (AP-2) which associates with the plasma membrane *phospholipid*

phosphatidylinositol-4,5-bisphosphate (PIP_2), stimulating the recruitment of clathrin protein at the site of the endocytosis; clathrin organizes for guiding the invagination of the vesicles and finally their internalization [14].

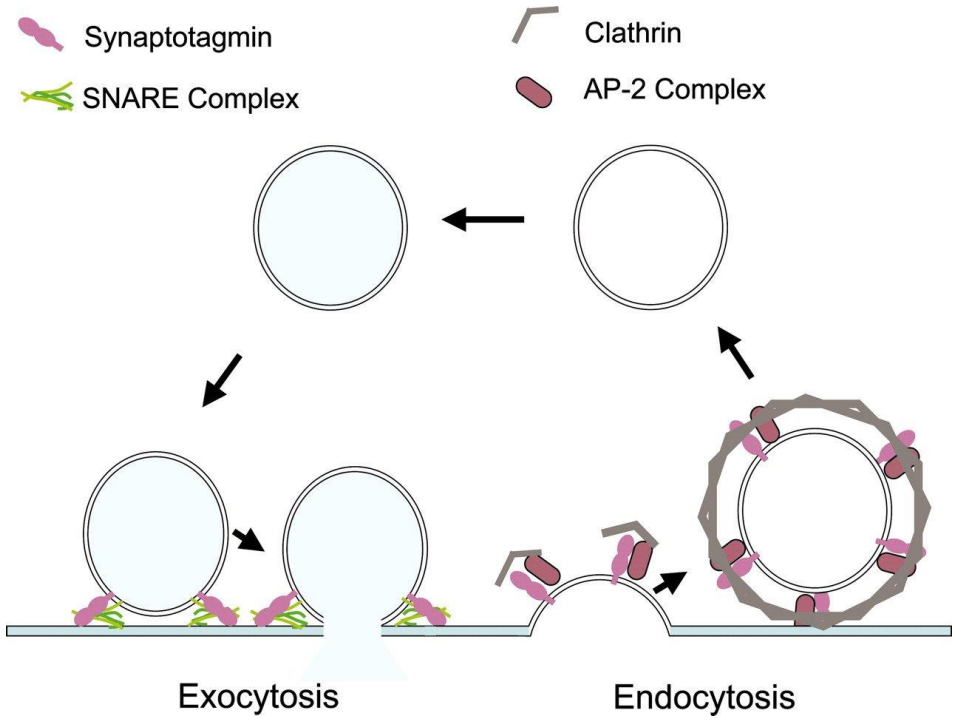

Figure 1.5 SNARE complex-mediated exocytosis and endocytosis. During exocytosis, synaptotagmin interacts with the SNARE complex promoting the exocytosis of the neurotransmitter, while it mediates the endocytosis of the vesicle when associating with AP-2 [15].

1.3.2 Receptor binding

The neurotransmitter previously released diffuses and couples with the postsynaptic receptors. There are two types of receptors:

- Ionotropic receptors: they are bound to ligand-gated ion channels, and by opening them, electric current flows and evokes a postsynaptic potential (PSP). The resulting PSPs are also called fast PSPs since they last about 20 ms [16], which is relatively a short time;
- Metabotropic receptors: they are G protein-coupled receptors able to activate second messenger systems, such as cAMP, cGMP, and Ca^{2+} [9], thus indirectly determining an intracellular event or ion channel opening. The transmitter which is

responsible for this indirect response is also called a neuromodulator, to distinguish it from a neurotransmitter, that binds to ionotropic receptors. The elicited PSPs are known as slow PSPs since the effectiveness of the resulting modulation is long-term;

If the current flowing through the membrane channels is depolarizing, we have an excitatory postsynaptic potential (EPSP), which makes the cell more likely to have an AP, whereas we have an inhibitory postsynaptic potential (IPSP) if it hyperpolarizes the cell, making the cell less excitable. EPSPs are mediated by two main receptors, the *N-methyl-D-aspartate receptor* ($NMDA_R$) and *α-amino-3-hydroxy-5-methyl-4-isoxazole propionic acid receptor* ($AMPA_R$). They are ionotropic transmembrane receptors, and their most important neurotransmitter is glutamate. In the genesis of the IPSPs, the major neurotransmitter involved is *γ-aminobutyric acid* (GABA) which binds to ionotropic $GABA_R$ [8].
These are the most important receptors for signal transmission, but there are many others, which are not being discussed here since the receptors described above are found to be playing the dominant role in synaptic plasticity.

1.4 Synaptic plasticity

One of the most fascinating hallmarks of the brain is neuroplasticity. Neuroplasticity refers to how neurons change in response to stimuli. These changes could be short-term if they last seconds to minutes, or long-term when lasting hours, days or even a lifetime. Plasticity generally occurs at the synapse level, that is why we call it synaptic plasticity, but other forms of plasticity have been also observed, e.g., within the neurons or other cell types such as astrocytes [17]. Many definitions of synaptic plasticity can be found in the literature, with the core concept being that synapses can be strengthened or weakened whenever their activity increases or decreases [18]. We name potentiation when the strength of the information flow is increased, and depression when it is reduced.
In this section, first, the mechanisms of synaptic potentiation and depression will be revised, to have a general idea about what they are and how they can arise. Secondly, we will deepen in Hebb's theory which describes the principles by which synaptic efficacy

could increase, and after that, we will see a particular type of synaptic plasticity, called spike-timing-dependent plasticity.

1.4.1 Long-term potentiation

In 1973, Terje Lømo and Tim Bliss were the first who tried to describe long-term potentiation (LTP) [19], thought to be at the basis of learning and memory. What they did was to stimulate unanesthetized rabbits at the synapse between the presynaptic fibers of the perforant path and the postsynaptic fibers of the dentate gyrus, and they recorded the PSP. The results showed that some high-frequency trains of stimuli (15-100 Hz) delivered multiple times at the presynaptic fibers can determine a long-lasting increase (hours) in the EPSP amplitude (Figure 1.6). This experiment was the first observation of LTP.

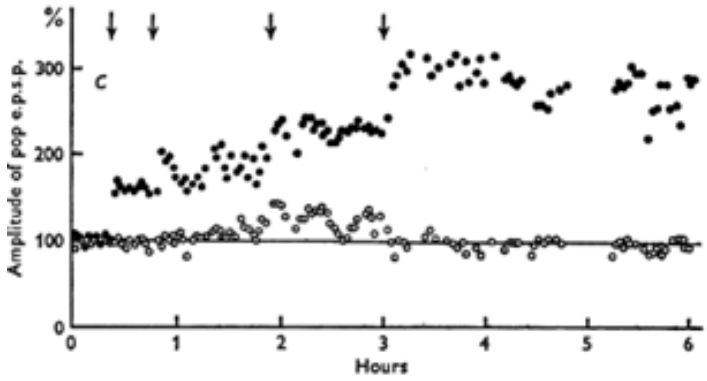

Figure 1.6 EPSP percentage amplitude change as a function of time at the perforant path-dentate gyrus. The control is represented with open circles and experimental pathway with filled circles. The arrows indicate the time instants in which the conditioning train stimulus is given (15 Hz for 10 s) [19].

After that, many studies have been carried out to understand the signaling pathways on which LTP depends.
First of all, it has been observed that LTP is characterized by some essential properties [20]:

- specificity: LTP is restricted to only the synapses which feature a strong stimulating input, and it does not spread to other synapses which are not receiving the stimulation (Figure 1.7a);

- cooperativity: the idea is that many small weak inputs converging to a single pathway can collectively depolarize the postsynaptic membrane if they are delivered together, and consequently, LTP is induced (Figure 1.7b);

- associativity: if a strong stimulation input of one pathway is paired with a weak input belonging to another pathway simultaneously, not only the former and stronger pathway will be strengthened, but even the weaker one (Figure 1.7c).

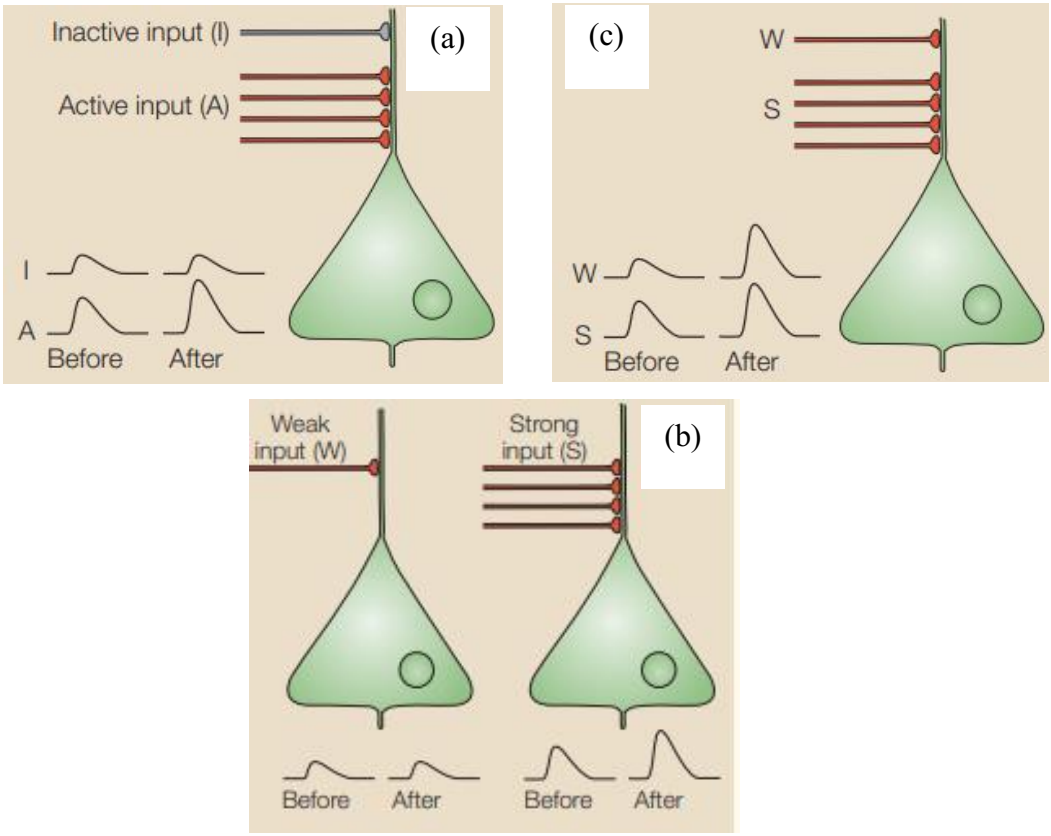

Figure 1.7 LTP properties. (a) Specificity. (b) Cooperativity. (c) Associativity [21].

Many mechanisms mediating LTP have been discovered, here we discuss the $NMDA_R$-dependent LTP mechanism [22] which has been identified in many regions of rabbit hippocampus:

1. $NMDA_R$ activation: glutamate binds to $AMPA_R$ and causes them to open resulting in Na^+ inward current leading to depolarization. Instead, $NMDA_R$ is normally blocked by Mg^{2+}; however, a strong stimulation provided by the release of

glutamate removes the Mg^{2+} block, and, since $NMDA_R$ is permeable to Ca^{2+}, Ca^{2+} intracellular concentration rapidly rises;

2. Ca^{2+} binds to *calmodulin-dependent protein kinase II* forming the complex CaMKII;

3. CaMKII phosphorylates $AMPA_R$ and increases its conductance. Moreover, CaMKII activates target proteins involved in the trafficking of $AMPA_R$; new $AMPA_R$ are inserted at the postsynaptic membrane, coming from an adjacent pool of $AMPA_R$. Both events will increase the evoked EPSP amplitude to the baseline stimulus.

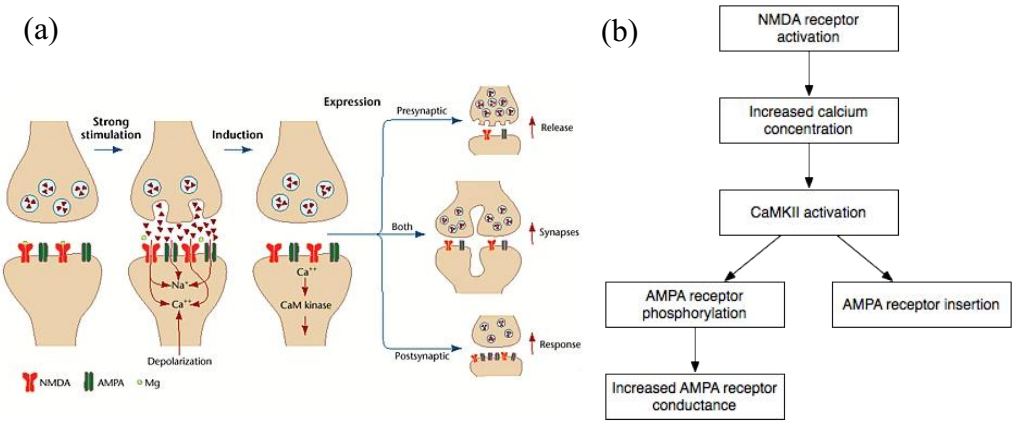

Figure 1.8 LTP routes. (a) Schematic diagram of one molecular mechanism of early LTP [23]. (b) Early LTP can be induced thanks to a strong stimulation and it can be manifested as an increase in neurotransmitter release, and insertion of new $AMPA_R$ [24].

These steps represent the early phase of the LTP (Figure 1.8a), which is independent of protein synthesis. A late and long-lasting response is mediated by gene transcription and translation (Figure 1.8b); as a result, structural changes become evident like the formation of new dendritic spines and the synthesis of new proteins involved in the maintenance of the new synaptic connections. An increase in the presynaptic synthesis of synaptotagmin and vesicle number results in enhanced neurotransmitter release, with a higher probability to evoke an EPSP [23]. Because of that, a connection from the postsynaptic to the presynaptic cell has to exist. Some authors believe in the existence of retrograde messengers which should be released by the postsynaptic cell and target the presynaptic

neuron to inform that LTP has occurred and elicit a modification in the presynaptic neuron [25]. The key signal could be the generation of back-propagating action potentials (bAPs), i.e., an AP that propagates from the AIS towards the dendrites, to distinguish it from the well-known AP along the axon. At the moment, bAPs represent a quite controversial topic, and further research should be carried out.

1.4.2 Long-term depression

In contrast with LTP, long-term depression (LTD) is a reduction in the transmission efficiency of a synapse, causing a decrease in the EPSP amplitude. That should not be intended as a negative condition, since neurons (but also astrocytes) can decide the functional synapses to strengthen, and weaken those who are not; otherwise, if the neurons reach the maximum limit of efficacy, the correct encoding of information will be prevented [7].

LTD has been mostly studied in the hippocampus and the cerebellum, and many patterns have been investigated, but most of them still need to be well-understood. All of the studies agree with the role of Ca^{2+} upon $NMDA_R$ activation by the glutamate neurotransmitter, like LTP, but what happens next is different (Figure 1.9). In the case of LTP, we observe a large and fast increase of the intracellular Ca^{2+} level induced by a strong $NMDA_R$ activation, which is responsible for triggering protein kinase CaMKII. In LTD, the $AMPA_R$ and $NMDA_R$ activations are weaker, and the resulting intracellular Ca^{2+} concentration is lower [26]. Unlike LTP, this event is shown to activate protein phosphatases, in particular, *protein phosphatase 1* (PP1), which is the major one beneath the postsynaptic membrane, and *Ca^{2+}/calmodulin-dependent protein phosphatase calcineurin* [27]. Calcineurin indirectly activates PP1 and triggers a signal cascade, which is not completely clear yet, causing the dendritic spines to shrink and the internalization of $AMPA_R$ via clathrin-dependent endocytosis [28], [29]. The reduction of the number of $AMPA_R$ decreases the postsynaptic neuron sensitivity to glutamate.

Another mechanism by which LTD can also be induced is through the dephosphorylation of $AMPA_R$ *serine-845* residue, which appears to reduce the $AMPA_R$ conductance [30]. The same conclusions related to the connection between post-presynaptic cells we arrived at in the LTP description could be addressed to LTD as well.

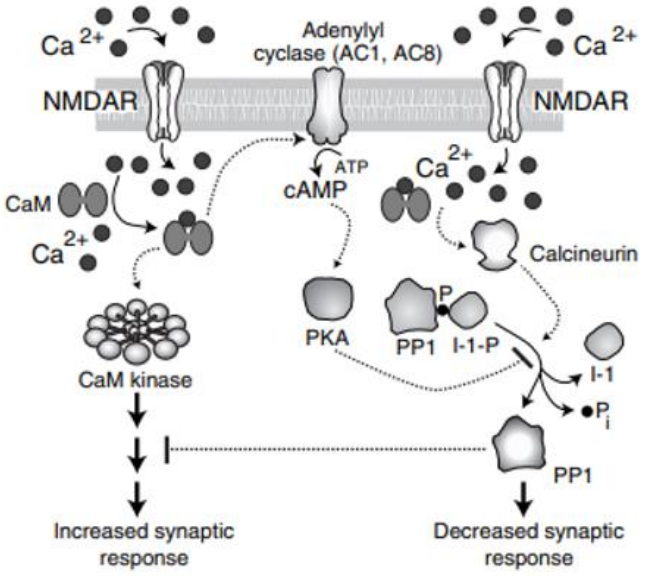

Figure 1.9 Representation of possible LTP and LTD pathways. High Ca^{2+} concentration (on the top left) causes not only the activation of CaMKII but also of cAMP which indirectly inhibits calcineurin, promoting LTP. On the other side, low Ca^{2+} concentrations induce the activation of calcineurin and PP1 leading to a decrease in the synaptic response. PP1 has an inhibitory effect on CaMKII preventing the CaMKII-dependent LTP mechanism [14].

1.4.3 The Hebbian theory

Many attempts have been tried to explain synaptic plasticity. How our brain processes and retains the information coming from environmental stimuli, is a question that can be addressed by Hebb's theory. Donald O. Hebb is considered by many the father of neuropsychology since he formed the foundations of research on learning and memory and bridged the gap between neurophysiology and psychology. According to Hebb, learning and memory are the results of three stages, corresponding to three postulates published in the seminal book *"The Organization of behavior"* (1949) [31].
The first and most cited postulate, representing the beginning of the whole process, states that:

> *"When an axon of cell A is near enough to excite a cell B and repeatedly or persistently takes part in firing it, some growth process or metabolic change takes*

place in one or both cells such that A's efficiency, as one of the cells firing B, is increased." [31]

The postulate explains the casual relationship underlying synaptic strengthening. Necessary coordinated activity between a presynaptic neuron, which fires first, and a postsynaptic neuron, which fires afterward, strengthens their connection; conversely, the connection would be weakened if the activity of the two neurons is uncoordinated. This last consideration has not been truly postulated by Hebb, but it was suggested and verified by subsequent studies and became an extension of Hebb's first postulate.

The second postulate concerns the slow development of cell assemblies upon repeated and strong series of stimuli; the cell assembly acts as a unified system, which means that a stimulus activating a certain pathway will reverberate activating a subsequent series of pathways [32]. This concept is also summarized as "*Cells that fire together, wire together*" [31].

The cell assembly can be imagined as the processing unit of thought, while the consecutive activity of cell assemblies forms a "phase sequence", the process that creates a complete mental representation of the stimulus previously received, providing the basis of the memory mechanism. This concept describes the third postulate [31] and sets out how neural information is integrated into the CNS.

Hebb's theory is not recent, however, it still has a great influence on the field of learning research, since neuroimaging techniques have shown the existence of such cell assemblies and their activation in working and recognition memory [33], [34].

1.5 Spike-timing-dependent plasticity

As described in the previous sections, Lømo and Bliss have demonstrated that hippocampal LTP can be induced by high-frequency (> 10 Hz) stimulation of the presynaptic fibers. Along the same trail, other researchers have also shown the same pattern, noticing that low-frequency (< 10 Hz) presynaptic stimulation rather drives LTD [35]–[37].

Other experiments have highlighted the importance of a new critical parameter, besides the frequency of the stimulation, which is the time correlation between presynaptic and postsynaptic activity. Hebb's causality described in the first postulate was already hiding this concept, that a defined temporal order between the presynaptic and postsynaptic spikes must be satisfied to induce LTP and LTD. This spike-timing-dependent form has been given the name of spike-timing-dependent plasticity (STDP). In 1983, Levi and Steward were the first who observed that LTP can be induced when the presynaptic spike occurs just before the postsynaptic response, while LTD can be elicited if the order is reversed [38]. At the end of the past century, many other groups found out that both the amplitude and sign of the EPSPs are strictly dependent on the time delay between the presynaptic and postsynaptic spikes on the scale of 10 ms [39], [40]. After that, other studies have tried to quantitatively characterize the synaptic plasticity as a function of time delay (Figure 1.10), discovering that LTP onto neocortical and pyramidal cells is induced by pre-leading-post spike activity within a 0-20 ms window, while LTD results from post-leading-pre spiking by 0 to 100 ms, depending on the considered neurons [41], [42]. The plot in Figure 1.10 (change in EPSP amplitude as a function of the time interval between the presynaptic spike and postsynaptic spike) is also called learning window, and it must be noticed that it is just one of the possible results of neuron stimulation, since the shape, amplitude, and sign primarily depends on the synapse which we are concentrating on. However, this is the typical shape that scientists tend to reproduce with excitatory neurons.

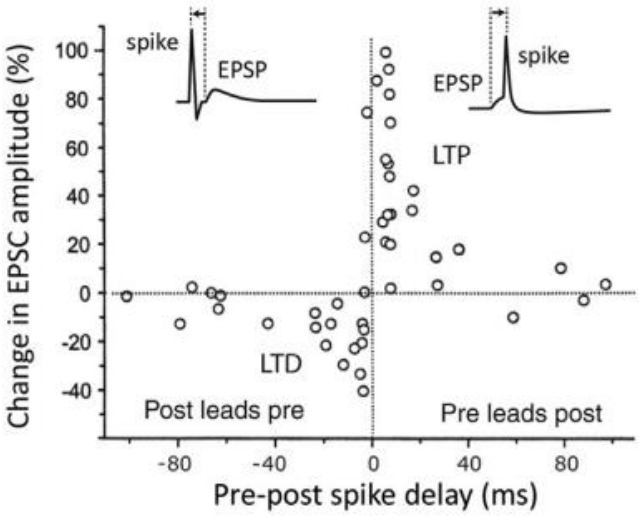

Figure 1.10 EPSP amplitude changes as a function of spike interval Δt. Positive Δt is the time between the postsynaptic and presynaptic spikes. For more details about the stimulation see [40]. Excitatory hippocampal neurons are used (one cell corresponds to one circle) and 60 spikes pairings are applied.

As described it is the Hebbian STDP, because Hebb's theory implements the causality concept: only coordinated synapses can be strengthened, which means presynaptic prior to the postsynaptic spike, while not structured synapses (or "non-causal" synapses) are weakened. Hebbian STDP has been observed in the majority of the excitatory synapses (excitatory presynaptic to excitatory postsynaptic neuron) in neocortical and hippocampal regions of the brain [39] however, it has also been noted by some authors that some excitatory synapses feature an opposite behavior (or anti-Hebbian STDP), i.e., LTP is induced by post leading presynaptic spike and LTD by the vice versa [43]. It has to be noticed that different synapses may show different STDP learning windows [44]. The Hebbian STDP is the oldest form of STDP discovered and consequently, most of the research has been done in this direction; however, much more study needs to be carried out to get a deep knowledge of this overall variety.

1.6 Microelectrode arrays for extracellular recordings

Electrophysiology can be studied either by intracellular or extracellular means. An intracellular recording is performed by puncturing the cell membrane with an electrode; this technique allows very high-precision measurements of numerous events inside and

across the cell, such as membrane potential, ion currents, and channel conductance. However, the invasiveness is the main drawback of this technique, which severely limits the experiment time up to maximum few hours, making it impossible if we want to study network activity in a cell population. To overcome this limitation, microelectrode arrays (MEAs) for extracellular recording started to spur, enabling long-term measurements of electrical activity in neural networks, both in vitro and in vivo.

MEAs have been extensively used in the last decades and they appear as a 2D arrangement of electrodes capable of both recording and stimulating electrogenic cells. The main advantages carried by MEAs are:

- Non-invasive recording;
- Long-term measurements (weeks to months);
- Multi-site simultaneous electrode analysis;
- Possibility to release stimulation;
- Small size (some mm^2), making it easy to handle inside incubators and on the lab bench;

Thanks to the advancements in microtechnology, MEAs can now be built in complementary-metal-oxide-semiconductor (CMOS) technology. This development has brought MEAs to the next step since the number of electrodes has passed from some hundreds to several thousand. These devices are also called high-density microelectrode arrays (HD-MEAs), because of the high number (thousands) of electrodes; the higher the number, the higher the resolution, which is necessary to reliably and individually locate the cells on the array.

1.6.1 Signal measurement

A HD-MEA is capable of measuring the current ion flows associated with the closest neuron. It must be clarified that an extracellular action potential (EAP) is different from the one that can be recorded using an intracellular probe. In Figure 1.11 intracellular and extracellular recordings at the level of the soma are compared. Generally, EAP amplitudes are three-fold smaller than intracellular action potential (IAP): in rats, if the latter is some millivolts order, the former can be some tens up to a few hundreds of

microvolts. The shape is also different, or rather opposite: an IAP is what has been described in Figure 1.2 and shown here in Figure 1.11; on the contrary, an EAP exhibits a large negative peak due to the fast inward current of Na^+ ions flowing away from the electrode towards the cell, and then a small positive peak corresponding to the slower outward current of K^+ ions directed from the cell to the electrode. The duration of an AP is almost the same, typically less than 2 ms [45], regardless of the mean by which it is recorded.

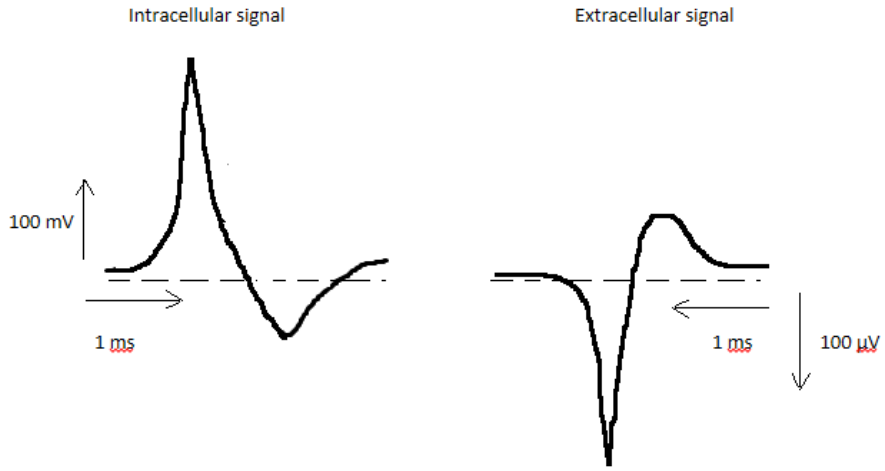

Figure 1.11 Comparison between intracellular and extracellular soma action potentials.

In general, the EAP amplitude depends on the electrode distance from the source as well as its relative position and direction of AP propagation; also, the size of the cell is important because larger cells yield higher AP amplitudes [45]. There are some aspects not directly related to the cell which should be considered, like the resistance of the extracellular space to current, the metal electrode/electrolyte interface, and, easier to control, the size of the electrodes. The size of the electrode is extremely important, just taking into account this factor, we would want to have electrodes as small as possible because larger electrodes tend to average the signal coming from multiple sources, and consequently, they lead to a decrease in amplitude. The EAP shown in Figure 1.11 is the one typically recorded, and initiated at the level of the AIS, but it has been demonstrated that dendrites are also capable of generating APs [46]. They can be easily recognized because their amplitude is smaller.

1.6.2 Signal quality

The most important requirements that HD-MEAs need to satisfy are the high spatio-temporal resolution and high signal-to-noise ratio (SNR). Noise can derive from different sources, the main contributors [47] are reported in Figure 1.12 and are:

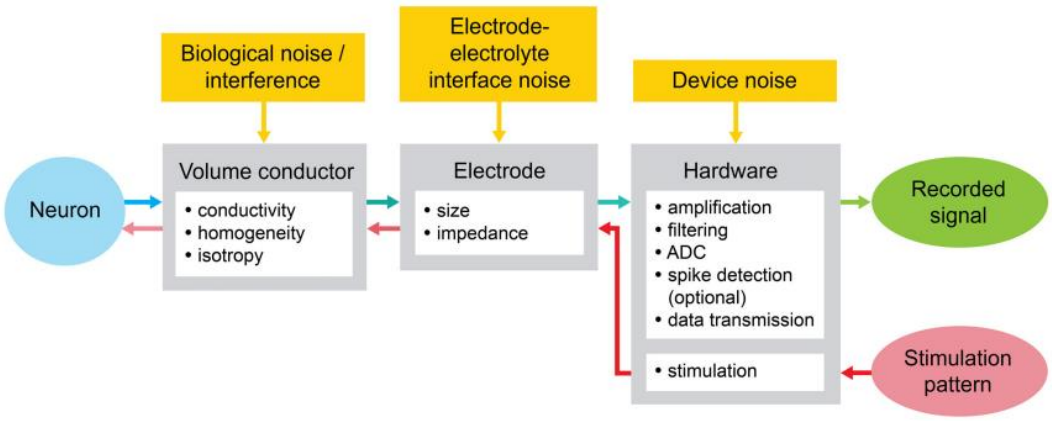

Figure 1.12 Main sources of noise in a MEA recording [47].

- Electrode/electrolyte interface noise, which can be canceled with a high-pass filter (below 10 Hz);
- Biological noise: e.g., distant firing neurons from the recording electrode (> 50 um) may corrupt the signal; if we use tissues, anisotropy can cause differences in the signal conduction;
- Thermal noise, which is directly proportional to the temperature and electrode impedance according to the equation [47]:

$$v_n = \sqrt{4 \cdot Re(Z_e) \cdot T \cdot K \cdot \Delta f} \quad (1)$$

  Where v_n is the equivalent thermal noise, T the absolute temperature, K the Boltzmann constant, Δf the noise bandwidth and $Re\,(Z_e)$ the real part of the electrode impedance. By selecting the electrode impedance, the thermal noise can be tuned to the desired need (with limits, since larger electrodes tend to average the signal coming from the surrounding cells) ;
- Power line interference (50-60 Hz): it can be handled by appropriate grounding;

- Circuitry noise from amplifiers (mainly associated with the front-end stage amplifier) and filters: the design of low-noise circuitry requires a balance between the area and power; lowering one of them inevitably makes the other increase.

These corruptions seriously affect the reliability of the results, consequently, it is mandatory to take all these factors in hand, to ensure a good signal quality for ease of spike detection which every study with MEA starts from.

1.6.3 Signal processing

Signal processing constitutes one of the main pillars of the whole system since it must ensure a reliable tool for the user to generally carry out his experiments

The general signal processing workflow [47] is:

1. Signal filtering in the AP band of interest (300 Hz – 6 kHz) to elevate SNR and remove the noise caused by the electrode-electrolyte interface noise or coming from biological sources, like the so-called local-field potentials (LFPs), which arise from synchronized synaptic currents summing altogether. LFPs are filtered out because they represent the synchronous activity due to all synaptic currents. Non-casual filters are used to steer clear of phase distortion.

2. APs detection: many strategies can be employed but the most widespread and easy to implement is amplitude threshold. An AP is marked every time the signal is above the defined threshold. Usually, the threshold is set at five times the noise standard deviation, but other measures of the baseline noise level can be used.

3. Spike sorting: this is the step that requires the highest computational effort. With the expression “spike sorting” we refer to the process of assigning each detected spike to its putative neuron. The spikes are structured in a high-dimensional space vector. Many steps focused on extracting spike features are needed, typically using principal component analysis to reduce the number of dimensions and keeping only the dimensions carrying most of the information. Spike clustering is then performed: spikes from the same neuron are grouped since they will be similar to

each other and dissimilar to those belonging to other neurons. Ideally, each cluster will represent one single neuron (called also a unit), and at the end, neurons are detected, along with their spike trains and "footprints", which are the averaged spike waveforms calculated for each neuron.

Since HD-MEAs have a large number of electrodes, the spike assignment becomes more reliable because spikes can be detected by more than one electrode. The high electrode density in HD-MEAs ensures that every neuron is detected, thus improving spike sorting [48]. An example is shown in Figure 1.13.

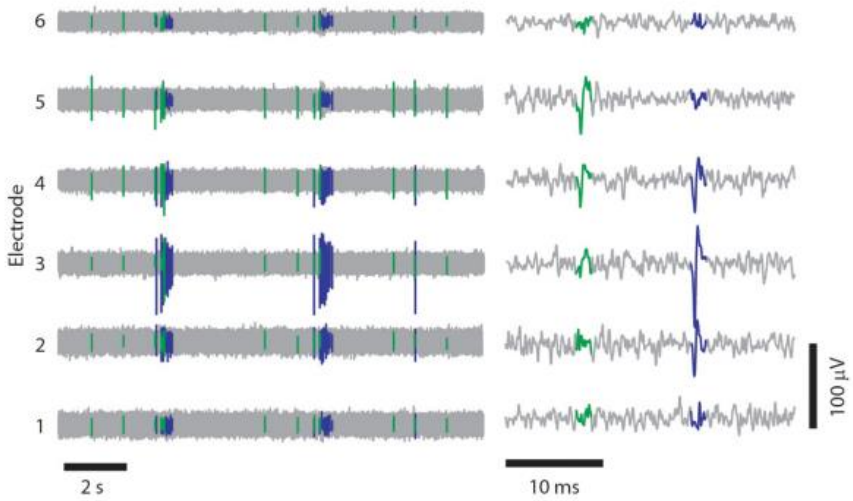

Figure 1.13 Signal recorded from six electrodes using a HD-MEA, where two neurons are detected. Electrode referred to as channel 4 does not allow for distinction between the two neurons. Only by using the information from the other channels, it is possible to separate them unambiguously [48].

1.6.4 Stimulation

The ability to electrically stimulate neurons is a fascinating capability able to expand the HD-MEAs potentialities in the neurosciences, picturing them as a powerful tool for the study of synaptic plasticity in neural cultures, restoring neural synapses, or even performing stimulation in closed-loop experiments. HD-MEAs provide flexible means to stimulate neurons by choosing the desired electrode subset and stimulus waveform, with the additional advantage that the stimulation electrodes can fast switch to recording mode as soon as the stimulus has been completely delivered.

A stimulus can be given in either voltage or current mode, with each modality having its pros and cons. Voltage mode is commonly preferred because it prevents unwanted electrochemistry, obviating Faradaic processes which may irreversibly damage the electrode. On the flipped side, it is not possible to know the generated current since it is dependent on the electrode impedance, which can undergo modifications during the electrode lifetime because of aging or simply by the application of some treatments, e.g., coatings. Instead, using current stimulation allows us to exactly know the amount of electric charge that is transferred, but not the electrode voltage, hence electrode degradation can occur.

Fixed the electrode material, waveform, amplitude, and duration of the stimulus must be thoughtfully chosen, to evoke the neuronal response.

It is not possible to know the exact parameters beforehand, since they depend on many factors, such as cell attachment to the electrode, the concentration of electrolytes in the medium solution, the impedance of the electrode, and others. However, some references do exist, the most recent one [49] has pointed out the monophasic negative and the biphasic positive-negative as the best voltage waveforms to trigger AP. The authors used a HD-MEA featuring 26 400 Pt electrodes at 17.5 μm pitch (Figure 1.14a), and stimulated the neurons at the level of the AIS, which is believed to be the most sensitive region to the stimulation where the highest EAP amplitude is generated [50]: by targeting the AIS, the lowest stimulation amplitudes can be used. They tested four different waveforms, at various conditions of amplitude and phase duration. Their results (Figure 1.14b) proved that monophasic negative pulse can efficiently evoke neural AP when the amplitude is above 160 mV_{pp} and phase duration greater than 100 μs. By using the same values, the biphasic positive-negative waveform is less efficient but still has a good stimulating capability, in comparison with the monophasic positive and biphasic negative-positive waveforms.

(a)

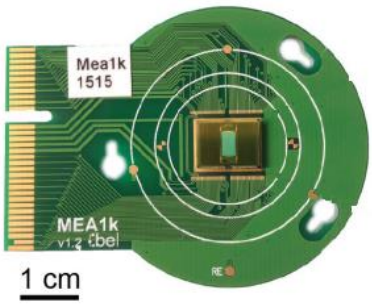

(b)

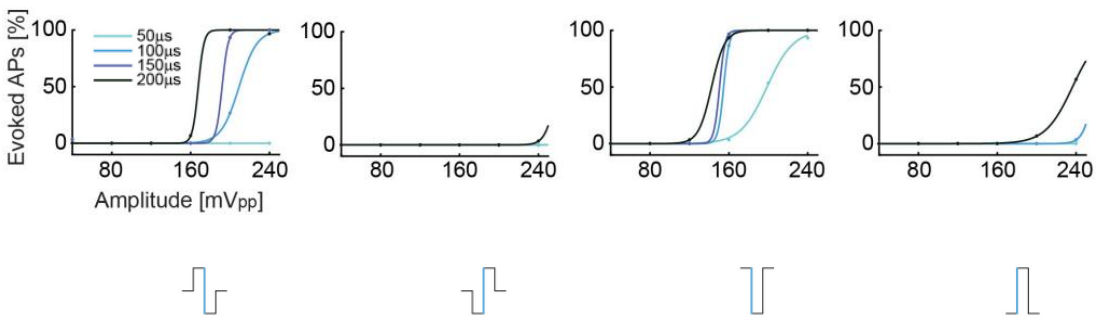

Figure 1.14 Stimulation efficiency of the HD-MEA consisting of 26 400 electrodes. (a) PCB-mounted MEA chip consisting of 26 400 electrodes used in [49]. (b) Stimulation efficiency using the MEA chip for the biphasic anodic-cathodic, biphasic cathodic-anodic, monophasic cathodic, and monophasic anodic waveforms [49].

2 Materials and methods

2.1 HD-MEA

A high-density microelectrode array (HD-MEA) providing 59 760 electrodes (3.0 x 7.5 μm^2) is used (overall sensing area: 4.48 x 2.43 mm^2). The electrodes follow a 332 x 180 layout at a 13.5 µm pitch; in particular, the device features 2048 AP recording units, 32 LFP recording units, 32 impedance measurement units, 32 current recording units, 28 neurotransmitter detection units, and 16 voltage/current stimulation units (Figure 2.1). For further information about the measurement setup and graphical user interface, the reader is referred to the appendix section (A.1 and A.2), while for the complete details about the device to the excellent existing paper presenting it [51].

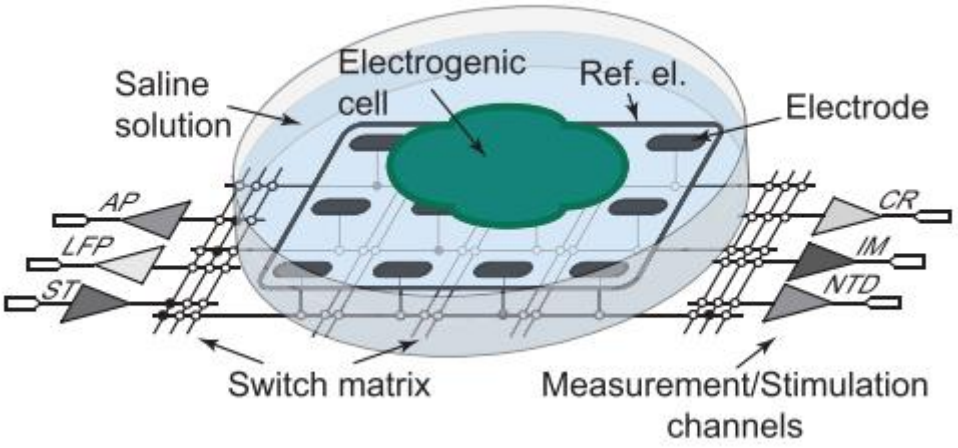

Figure 2.1 Device conceptualization with its AP, local field potential (LFP), neurotransmitter (NTD), impedance (IM), and stimulation channels (ST) [51].

2.2 Packaging

In order to stabilize the bond wires, the high viscosity epoxy EPO-TEK ® 353-ND-T 8OZ (Epoxy Technology Inc., Billerica, MA, USA) is selected. Kit part A and kit part B are mixed in a ratio of 10:1 and the epoxy is dispensed with a 3 mL syringe through a 22-G needle; the HD-MEAs chips are then baked in the oven at 80 °C for 1 h and let cool down at room temperature for 30 min. A 35 x 10 mm polycarbonate ring (Greiner Bio-One GmbH, Frickenhausen, Germany) is fixed with superglue (Pattex, Henkel, Dusseldorf, Germany**)** above the array for creating an enclosed space in which cells can accommodate**.** Kit part A and kit part B of epoxy EPO-TEK ® 353-ND (Epoxy Technology) are mixed and the resulting mixture is degassed for 30 min. The epoxy is applied to cover the area within the ring outside the electrodes with a 3 mL syringe and 21-G needle; the devices are finally baked in the oven at 80 °C for 1 h, then the temperature is ramped up to 150 °C for another 1 h and the chips are let to cool down at room temperature overnight. The epoxy serves for electrical isolation as well as protects the cells from aluminum: in fact, a possible release due to contact with the physiological medium may be harmful to the cells and needs to be avoided, since aluminum would be released because of some corrosion processes.

2.3 Platinum-black deposition

The chips are treated with plasma oxygen for 30 s setting 0.4 mbar pressure and 50 W power output, using a plasma generator system (Diener ATTO, Diener electronic GmbH & Co. KG, Ebhausen, Germany)**.** This step prepares the chip surface for the Platinum-black (Pt-black) electrodeposition. Pt-black plating is fundamental since it reduces electrode impedance (30-40 fold reduction [52]) and thus leads to an increase in the SNR.

The procedure is as follows. A platinum wire, as the counter electrode, is immersed in the working solution, consisting of 0.7 mL 100 mM hexachloroplatinic acid (Sigma-Aldrich, Saint Louis, Missouri, USA), 0.03 mL 0.3 mM lead (II) acetate anhydrous (Honeywell, Morris Plains, New Jersey, USA), and 9.27 mL deionized water. Since the chip electrode area is 1.5 mm^2, a 20-30 mm length for a 100-µm-Ø wire is suitable, as the counter electrode should be at least 10 times as large as the whole electrode area. A current of 400 µA is then applied for 30 s using a current sink generator to coat simultaneously all the electrodes, by wiping at the same time the chip with a cotton stick to ensure a more uniform

coating. The procedure is then repeated in order to obtain a sufficient deposition. Similarly, the reference electrodes are coated using the same setup, with a current of 200 μA applied for 30 s; during the process, the solution is stirred with a pipette to move the bubbles away from the chips. In order to evaluate the importance of Pt-black deposition in noise attenuation, the power spectral density (PSD) of the signal is calculated by exploiting the periodogram, i.e., using a rectangular window having the same length of the signal. The PSD is calculated on the signal extracted from one channel from a chip with Pt-black and a chip without it. The recording is done by pouring 2 mL of PBS on the chips.

2.4 Cortical cell culture

The chips are sterilized with 70 % EtOH for 40 min and rinsed three times with deionized water. The electrodes are treated with 10 μL 0.05 % (w/w) poly(ethyleneimine) (PEI) (Sigma-Aldrich) in borate buffer pH 8.5 (Chemie Brunschwig, Basel, Switzerland) and left for 40 min in the hood at room temperature. This step increases the hydrophilicity of the substrate and enhances cell adhesion. PEI is removed with a vacuum aspirator and the chips are rinsed three times with sterile water, which is taken away by the vacuum aspirator as well. Next, 10 μL 0.02 mg mL^{-1} laminin (Sigma-Aldrich) in Neurobasal medium (Thermo Fisher Scientific, Waltham, USA) is dropped over the electrodes, and the chips are covered with a 35-mm-Ø lid (Greiner Bio-One GmbH). The devices are placed in a 100-mm-Ø Petri dish along with a small 35-mm-Ø Petri dish (Greiner Bio-One GmbH) filled with water to prevent evaporation of laminin, and they are incubated for 30 min at 37 °C.

Cerebral cortices are extracted from Wistar rats E-18 and dissociated in 2 mL 0.25 % trypsin-EDTA (Thermo Fisher Scientific) for 20 min at 37 °C. The cortices are harvested and placed into 2 mL Neurobasal medium to induce trypsin neutralization; the mixture is then triturated by drawing up and dispensing out with a pipette at least 15 times. A 40-μm cell strainer is used for filtering large debris. The primary cortical cells concentration is measured with a hemocytometer (Sigma-Aldrich) by mixing 5 μL of the suspension and 5 μL of 0.4 % Trypan blue (Sigma-Aldrich). The suspension is then diluted with Neurobasal medium in order to have 30,000 cells/device which are seeded in a 10-μL drop on the active array. The chips are incubated to allow cell attachment for 30 min at 37 °C and then, 2 mL of plating medium is added, comprising of 450 mL Neurobasal (Thermo Fisher Scientific),

50 mL Horse Serum (Thermo Fisher Scientific), 10 mL vitamin B-27 (Thermo Fisher Scientific) and 1.25 mL GlutaMAX (Thermo Fisher Scientific). For the entire duration of the experiments, the cells are maintained inside the incubator at 37 °C, 9% O2, 5% CO2, and 65% humidity. Twice a week, 1 mL of the medium is replaced with the maintenance medium, consisting of 49 mL Brainphys (StemCell Technologies, Vancouver, Canada), supplemented with 1 mL 50X NeuroCult SM1 (StemCell Technologies) and 100 µL 10,000 U mL^{-1} Penicillin-Streptomycin (Thermo Fisher Scientific). The cells are cultured on the top-centre of 10 chip arrays, carried on in parallel.

All the experiments are performed following the protocols approved by the Basel-Stadt veterinary office, in accordance with Swiss Federal Laws on animal welfare.

2.5 Spontaneous electrical activity characterization

In order to carry out the stimulation and record the signals from the electrode array, custom-made software is used. Every part of the measurement setup going into the incubator is sterilized with 70% EtOH for 40 min and dried in the hood within the laminar flow.

The spontaneous neuronal activity is recorded at days in vitro (DIV) 7 and DIV 14, waiting for the cell growth and synapse establishment. A scan recording is performed in order to explore the whole surface of the active array; the scan is a concatenation of ten different recordings, each one obtained from a random configuration of electrodes (2048 channels). Each recording lasts 30 s, consequently, the whole duration of the scan is approximately 5 min. Cell activity can be estimated after measuring the peaks calculated by each electrode and considering their average peak amplitude from the raw signal. The recorded data is amplified with a gain of 1024, and sampled at 20 kHz, while the threshold for peak detection is 5 times the median absolute deviation of the noise (MAD).

After the cells have started to be functional, a high-density block of electrodes is used for recording a region of the chip with high-precision, where neurons are likely located. The scan helps to give a rough idea of where neurons are located. The signals, recorded for approximately 120 s are pre-processed using a band-pass filter with cutoff frequencies 300 Hz - 6 kHz; then, spikes are detected on each electrode every time the signal amplitude is higher than 5 times the MAD of the noise. The spike sorter Tridesclous, implemented in

Python (working in Jupyter Notebook environment running the Python-based SpikeInterface module), is chosen to assign each spike to the belonging neuron. MATLAB is also used for additional post-processing. The data is processed and spikes are sorted using the aforementioned method to identify putative neurons on the chip array. For further details about the parameters, and how the algorithm extracts the neurons from the spikes, the reader can look at the online documentation of Tridesclous package [53]

Once spike sorting is completed, putative neurons can be characterized by using the tools implemented in the SpikeInterface module [54]. Raster plot of the spike trains and waveforms of the APs are computed. Waveforms of the APs are extracted by taking the signal 3 ms and 4 ms before and after the peak respectively. Also, templates can be obtained from the extracted waveform: a template can be seen as the average waveform of the action potentials on a particular channel for a specific neuron, resulting from various steps of signal processing aimed at removing the noise and ending up with an ideal waveform that can characterize univocally that neuron. Inter-spike interval distribution is also calculated using a 100 ms window and 1 ms bin to establish if the neuron violates the refractory period when it fires.

Cross correlogram (CCG) analysis is performed to identify the potentially connected neurons, with the aim of stimulating afterward only pairs of likely connected neurons. CCG is computed using a 100 ms window divided into bins of 1 ms each. The reference and the target neuron spike trains are aligned, and the window is centered on each spike of the reference neuron; the number of spikes of the target neuron falling in every bin is calculated and the result is plotted in a histogram chart by summing all the bin counts in each window. Then, the result is normalized by dividing by the total number of spikes of the reference neuron to obtain the spike transmission probability (See appendix A.3 for a better understanding of the CCG basis).

2.6 Stimulation in PBS

Although previous experiments aimed to assess which waveform, amplitude, and duration of the stimulus able to effectively trigger AP have been previously reported, some trials are required to be performed with this new device. According to various studies, the neuronal compartment shown to be the most sensitive to stimulation is the AIS. Consequently, to stimulate a neuron the electrode to be selected is the one showing the

highest voltage amplitude, i.e., nearby the most sensitive region, which is likely situated underneath the AIS. In this thesis, only voltage stimulation is considered, because it features a lower probability to cause cell damage than current mode stimulation.

For being sure that a predefined pulse is correctly delivered to the cells without any errors, it is necessary to study the stimulation when it is not applied to any neurons. In particular, the stimulation is performed in PBS, by filling up the chip with a volume of 2 mL. The waveforms investigated are the monophasic negative and biphasic positive-negative (Figure 2.2), which successfully evoked APs in the reference paper involving an HD-MEA with 26 400 electrodes [49]. The amplitudes and phase duration of the pulses are listed in Table 1. The pulse is generated using on-chip digital-to-analog converters (DACs) and applied to the desired electrode using a voltage stimulation buffer. The recorded signal is amplified using a gain of 32 in order to avoid saturation of the amplifiers and every pulse is sent 5 times with a frequency of 1 Hz. (See Appendix A.2 to look up the workflow for doing a signal recording and delivering a stimulation pulse)

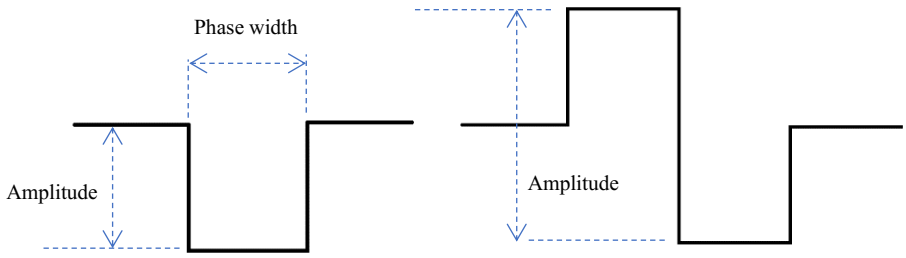

Figure 2.2 Stimulation waveforms tested. (a) Monophasic negative waveform. (b) Biphasic positive-negative waveform.

Pulse shape	**Amplitude (mV_{pp})**	**Phase width (µs)**
Monophasic negative	10, 20, 30, 40, 50, 100, 200, 300, 400	200
Biphasic positive-negative	10, 20, 30, 40, 50, 100, 200, 300, 400	

Table 1 Stimulation pulses tested.

Availability of materials

All the Python scripts for signal processing can be reached at the following link: https://github.com/alessandroforastiere/alessandro. The SpikeInterface suite can be reached at the link: https://github.com/SpikeInterface.

3 Results

3.1 Packaging and Pt-black deposition

A chip before and after the packaging is shown in Figure 3.1. The active electrode array is not coated with epoxy since it is where the cells are plated, while all the surrounding area is, to protect the cells from toxic elements that could be released from the chip in the medium solution.

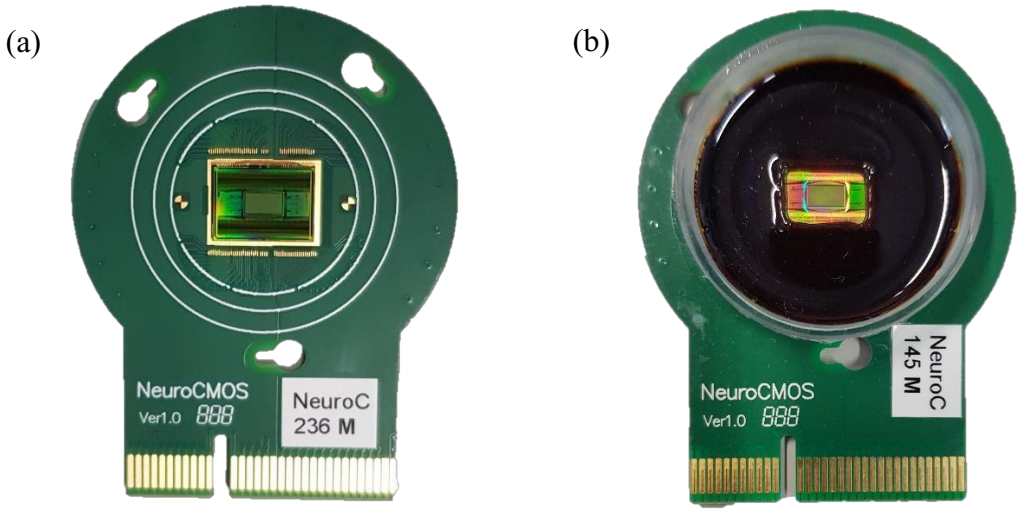

Figure 3.1 Photographs of the 59 760 electrodes device. (a) Device before packaging. (b) Device after packaging: note the presence of the ring for accommodating the cells and the epoxy EPO-TEK ® 353-ND which becomes dark after reticulation.

In Figure 3.2a and 3.2b electrodes before and after Pt-black electrodeposition are shown.

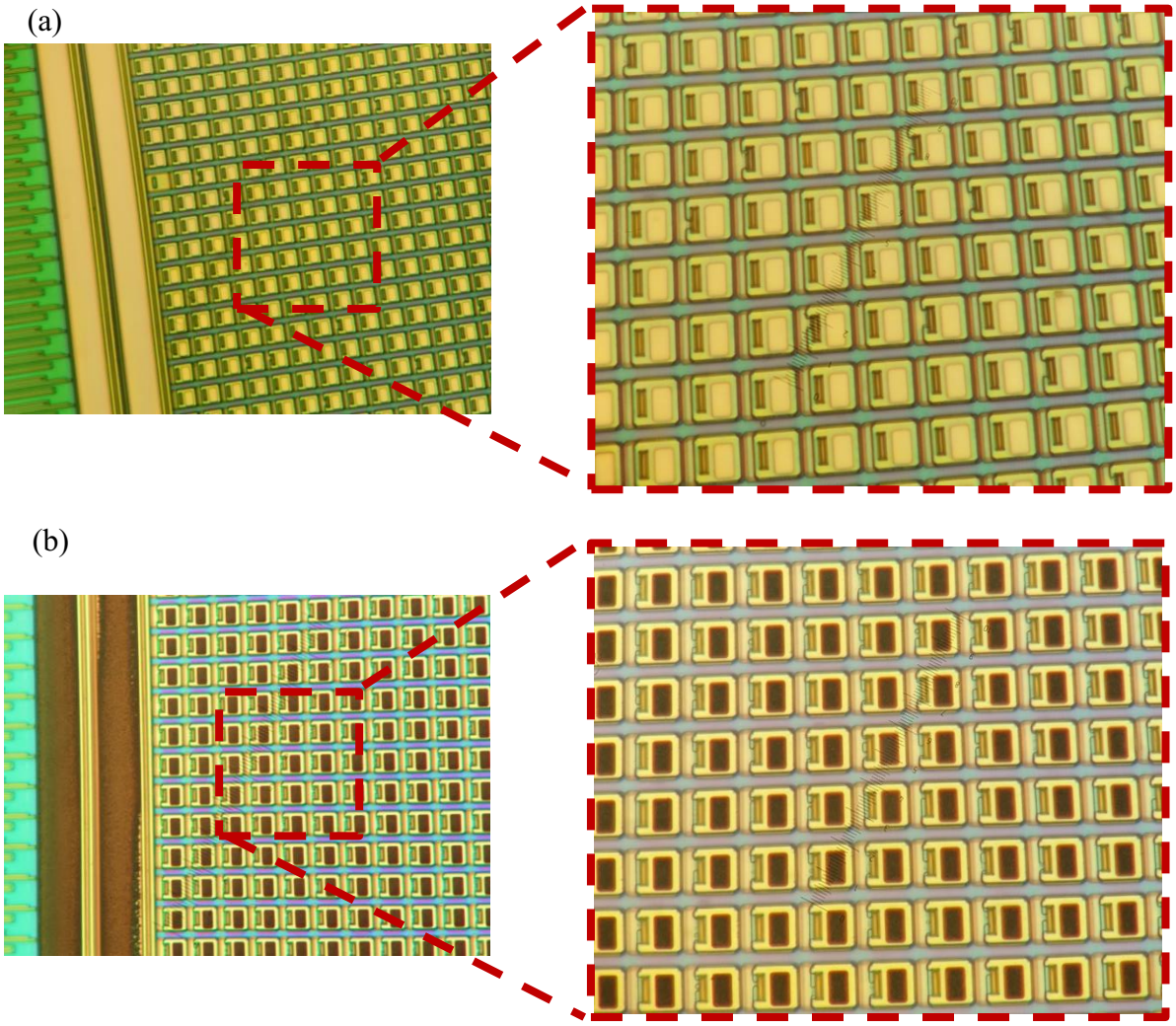

Figure 3.2 Pt-black deposition. (a) Electrodes before the deposition. (b) Electrodes after the deposition (the current is applied twice for 30 s). Pictures taken with a Leica MS5 microscope.

The picture displays a uniform deposition which is beneficial for achieving a high SNR by impedance reduction and recording a good quality signal. Moreover, the Pt-black deposition increases the surface area of the electrodes, thus the cells have a larger available area for their attachment.

By measuring the PSD from the signal of one random electrode, when the chip works just in presence of PBS solution and comparing the two cases, with and without Pt-black deposition (Figure 3.3), we can experimentally observe a reduction of the PSD associated with Pt-black coating of 93.6%. This is beneficial since we are only measuring noise and the coating helps reduce its power, and consequently the noise itself.

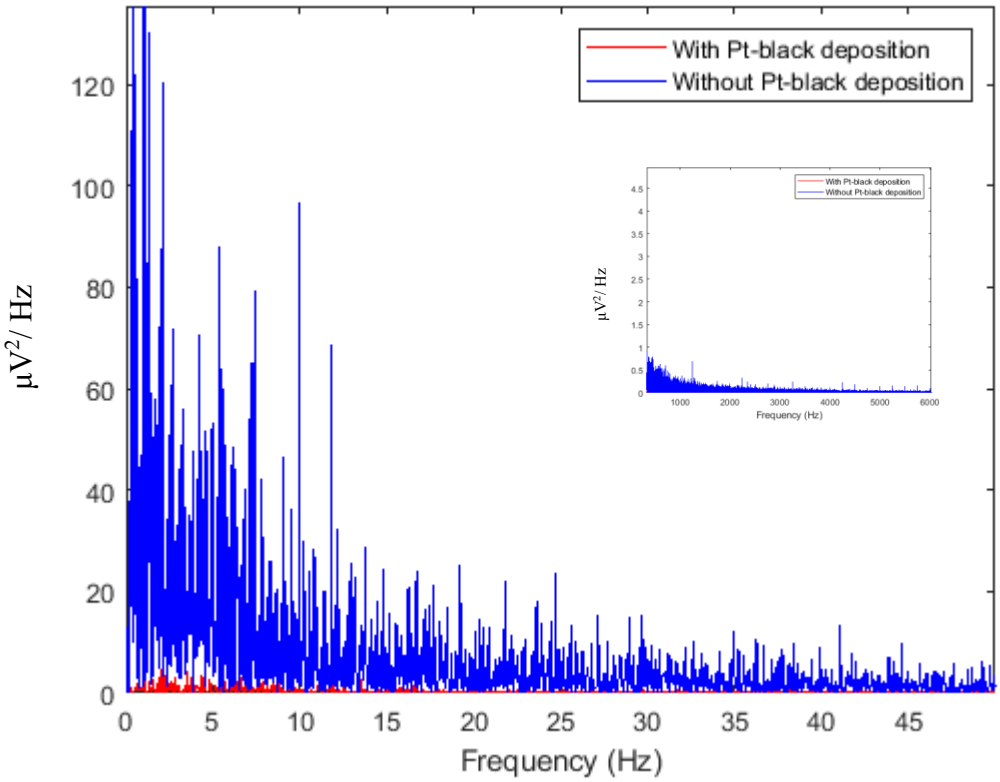

Figure 3.3 Power spectral density of the signal recorded in PBS, with and without Pt-black deposition..

3.2 Characterization of HD-MEA stimulation in PBS

In order to assess the capability of the system to reliably deliver a certain pulse having a predefined waveform, voltage amplitude, and phase duration, stimulation in PBS is carried out. First, monophasic negative pulses with phase time 200 µs are delivered. The signal is measured using the same stimulation electrode. All the pulses are shown in Figure 3.4a. As we can see, clipping occurs when the 20 mV-threshold is overcome; this should not happen since the supply voltage is 2 V and the gain 32; moreover, the more the amplitude is increased the more a new opposite waveform emerges after the pulse has been delivered. This phenomenon should not happen as well. The same can be observed by sending biphasic positive-negative pulses with a phase time of 200 µs (Figure 3.4b).

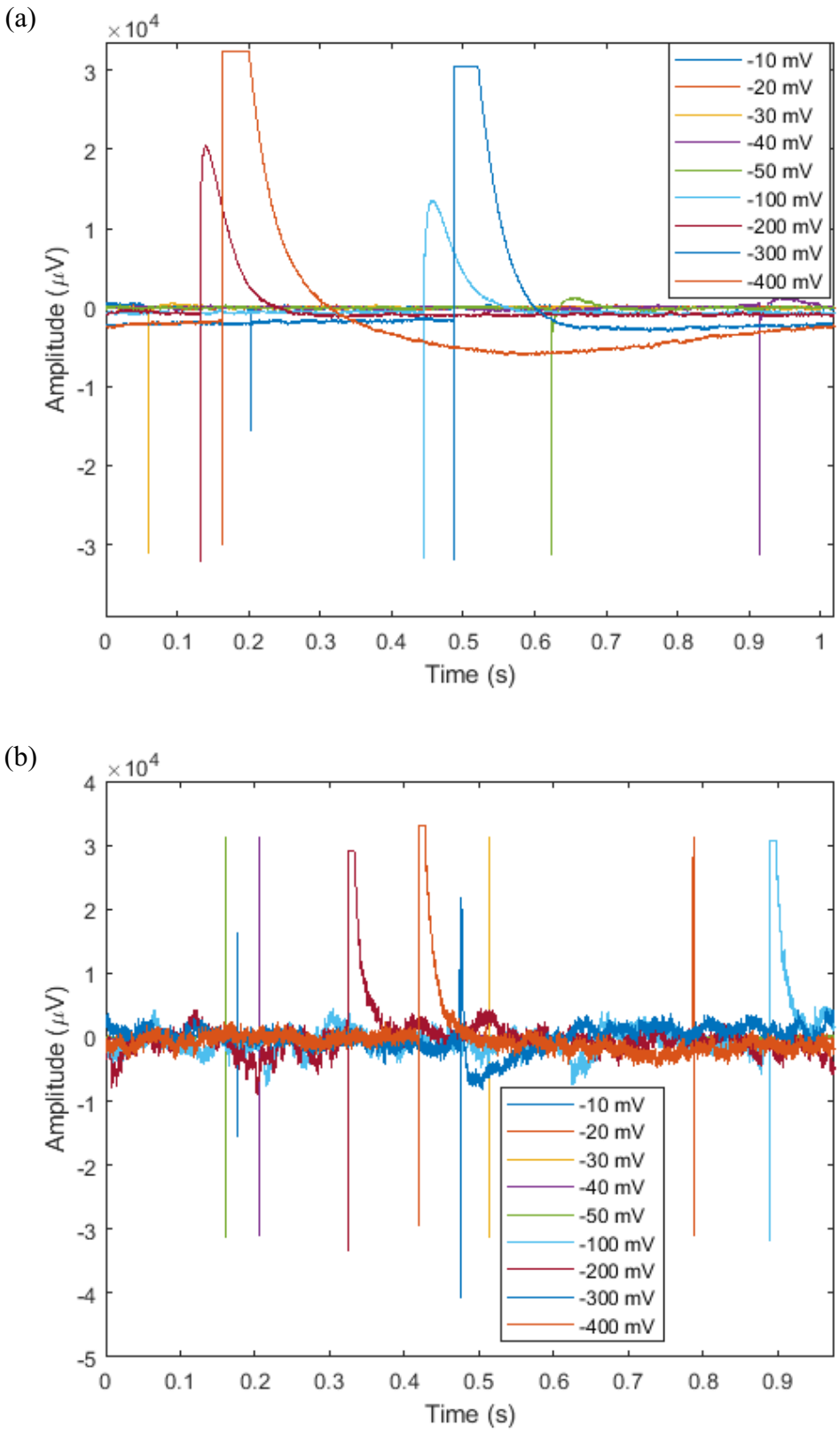

Figure 3.4 Monophasic and biphasic pulses for different amplitudes and phase duration 200 μs. (a) Monophasic negative. (b) Biphasic positive-negative.

Only a 10 mV-pulse does not cause saturation of the amplifiers, although we measure an amplitude that is slightly higher than 10 mV; this also happens when a 20 mV_{pp} biphasic pulse is delivered.

Regardless of that, looking at only waveforms not clipped (i.e., 10 mV), waveform and duration are satisfied, both in monophasic (Figure 3.5a) and biphasic (Figure 3.5b), with a small amplitude difference from the ideal value.

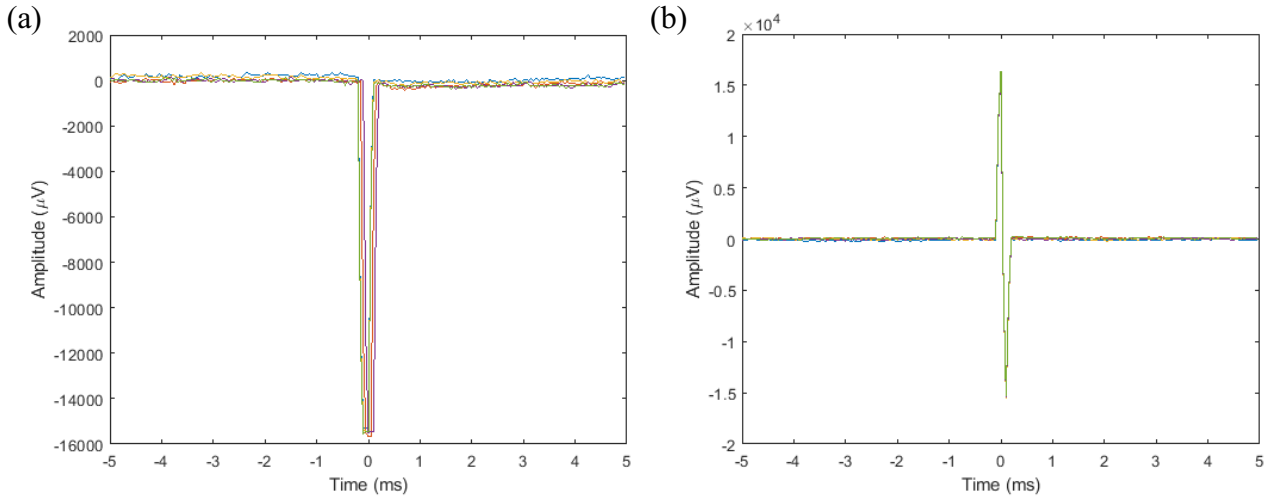

Figure 3.5 Recording after sending monophasic and biphasic stimulation pulses that do not cause saturation. (a) Five overlapped monophasic negative pulses with amplitude 10 mV, phase time 200 μs. (b) Five overlapped biphasic positive-negative pulses with amplitude 20 mV_{pp}, phase time 200 μs.

It would be interesting to know if the bigger amplitude of the signal is effectively due to the electrodes. For doing that, a biphasic positive-negative stimulation pulse is delivered and measured with an oscilloscope, by keeping the electrodes disconnected from the stimulation unit. Figure 3.6 shows that the test pulse, with amplitude 500 mV_{pp} and phase time 15 μs, has the correct amplitude this time, meaning that the phenomenon happening before could result from the not accurate settings of the amplifiers.

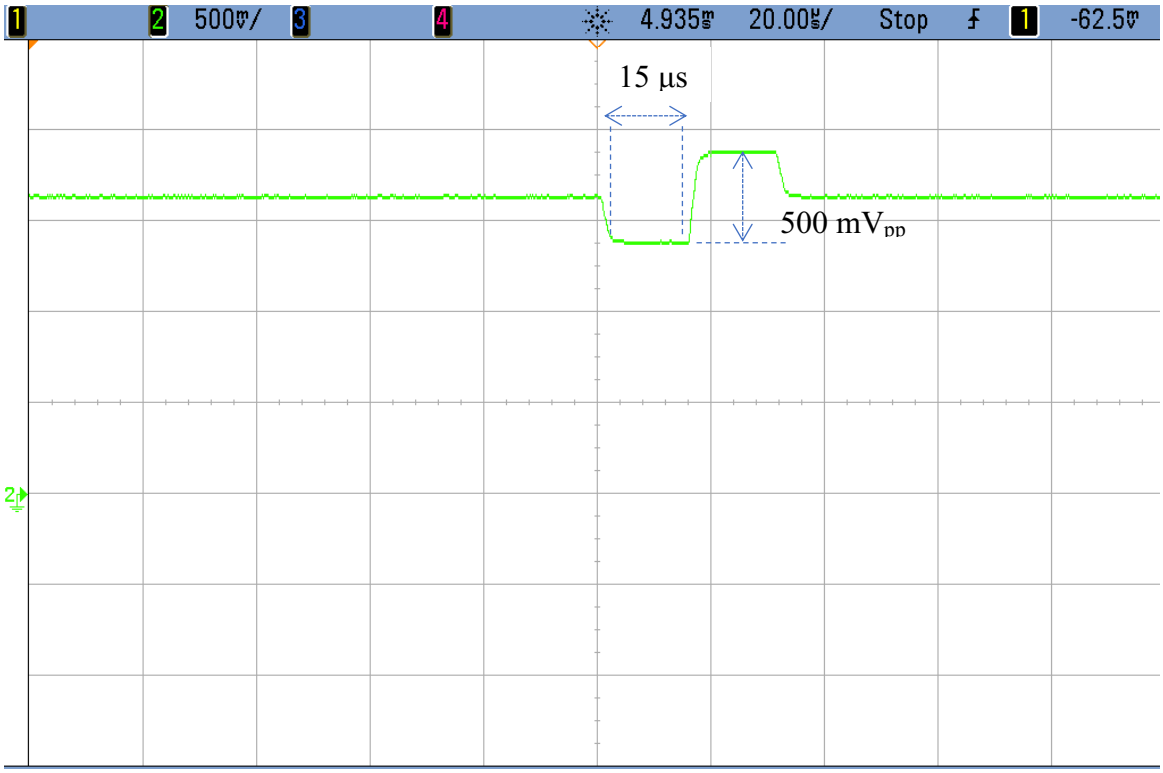

Figure 3.6 Biphasic positive-negative pulse with amplitude 500 mV_{pp} and phase time 15 µs. The pulse is recorded by using an oscilloscope (Agilent Technologies), with the stimulation unit and the electrodes disconnected (oscilloscope connected to the output).

3.3 Electrophysiological characterization

Following, the electrophysiological characterization of a neuron culture is described for one chip.

3.3.1 Scan activity

First, a scan recording is performed at DIV 7 to check the activity of the cells. From the results in Figure 3.7, we can notice there is no electrode, which measures at least one potential spike. Thus, the cell activity can be considered absent on the whole electrode array, and more days are required to see some functional growth.

Scan recording is therefore repeated at DIV 14. In this case, the frequency of the peaks is measured for each electrode on the array: looking at Figure 3.8, the distribution of the peaks is quite uniform, probably meaning that the cells have occupied most of the array's area.

Along with the peaks, the average peak amplitude is calculated and shown in Figure 3.9. Most of the electrodes show a low average peak amplitude since amplitudes range from 20 to 75 µV (absolute value), which is inferior to the hundreds of microvolts that we can grasp from the literature.

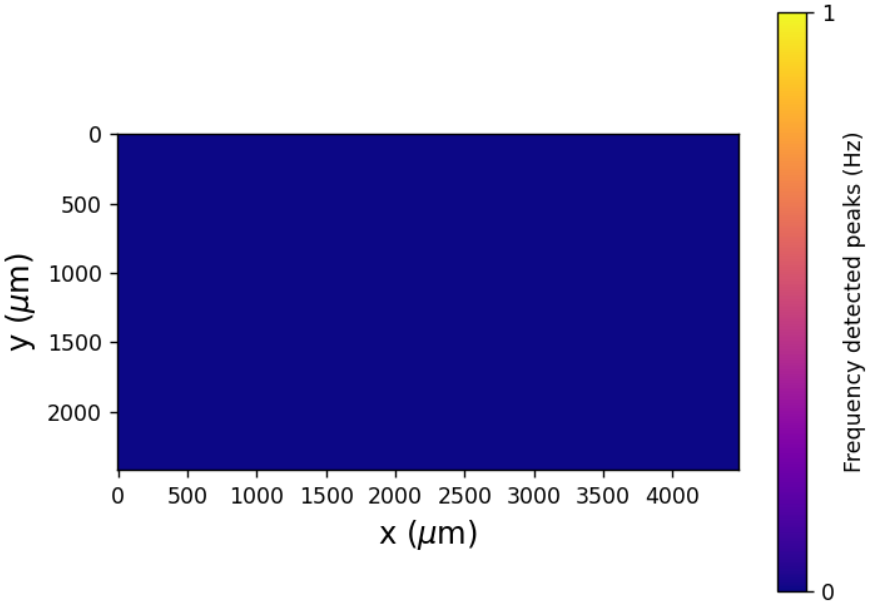

Figure 3.7 DIV 7 Activity scan: frequency of the peaks detected by each electrode on the active array.

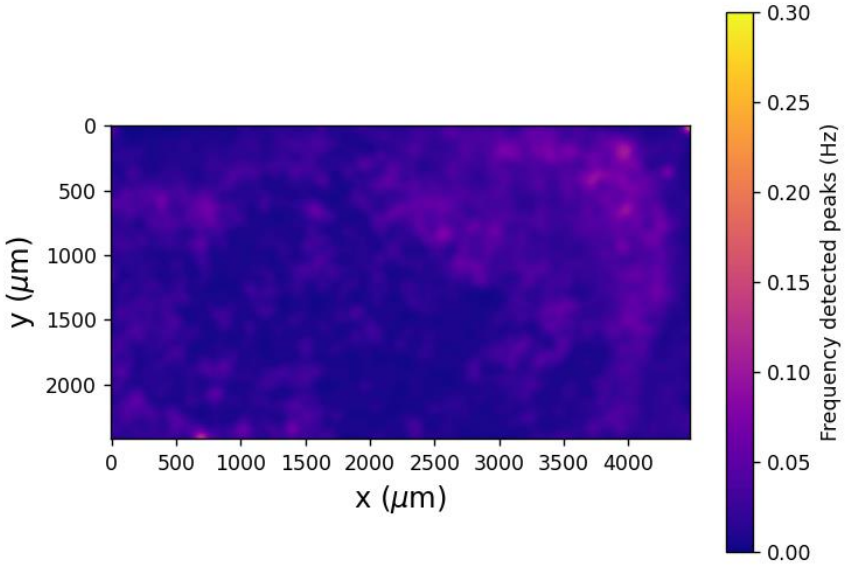

Figure 3.8 DIV 14 Activity scan: frequency of the peaks detected by each electrode on the active array.

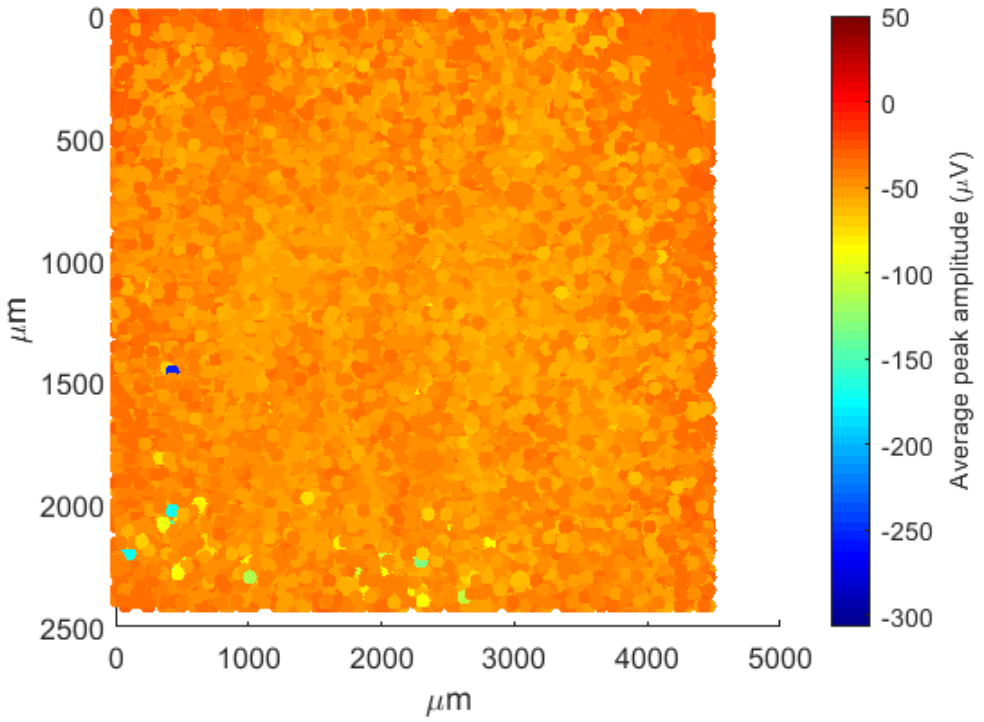

Figure 3.9 DIV 14 Average peak amplitude scan. For each electrode, all the peaks above 5 MAD are averaged.

However, although related to a few electrodes, we can start seeing potential cell activity looking at the bottom of the array where 100 μV or higher is measured. That could not necessarily be an indication of action potential detection, but simply a higher noise level which could distort the results since borderline peaks are marked as action potentials while they are actually due to noise. To check this, we can look at the signal at the electrode recording the highest potential (Figure 3.10a and 3.10b). The figures clearly show one peak which is a true action potential and not an error due to the noise. Moreover, the order of magnitude is similar to the one observed in the literature for extracellular recording, i.e., hundreds of microvolts.

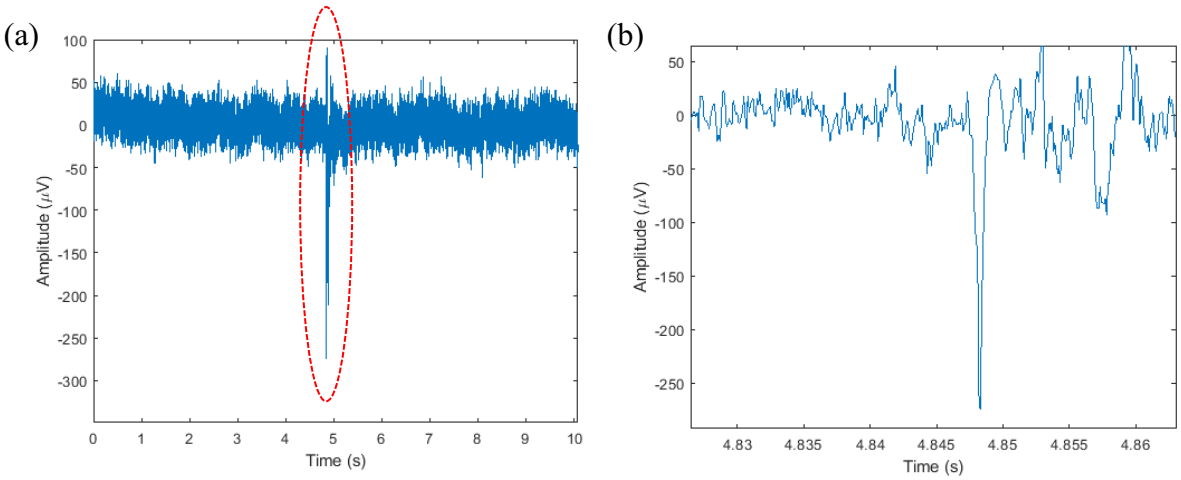

Figure 3.10 Signal recorded in the region where the highest potential is observed in average peak amplitude scan. (a) The whole recording shows a sharp peak. (b) Enlargement of the region where there is a peak: one noticeable AP with amplitude up to 250 μm can be observed.

3.3.2 Spike sorting

If we want to detect some neurons with the highest degree of reliability, recording from a random configuration of electrodes is not sufficient. For this reason, a so-called "high-density" block of electrodes (consisting of 2025 electrodes) is chosen, in which the distance between each electrode and the adjacent one is 13.5 μm, i.e., the electrode-electrode distance. Measuring the signal from lots of electrodes should improve the spike sorter's capability to differentiate the action potentials belonging to one neuron from the ones of another neuron. This block is typically "positioned" in the center of the array or nearby (where the peaks are concentrated or the amplitude is sufficiently high) since, having plated the cells in that position, we expect a higher probability to measure some activity there and not at the borders of the array. In Figure 3.11a and 3.11b, the high-density electrode configuration map is displayed.

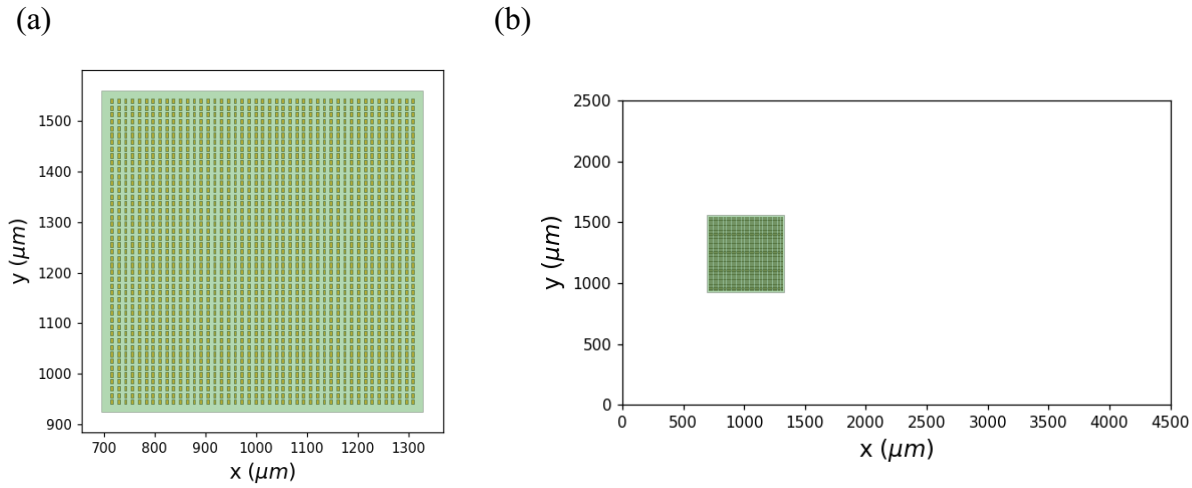

Figure 3.11 Electrode map configuration. (a) High-density electrode map configuration (2025 recording channels). (b) Map shown with the whole active array references.

Spike sorting is then computed using that map configuration at DIV 17. Here, in Figure 3.12a, the detected units (or neurons) are shown, in particular, the unit template (average waveform) at each electrode is plotted in the radius of 50 µm from the electrode measuring the highest potential for that neuron. In Figure 3.12b, it is represented a zoom-in of the templates of one unit: the soma should be located where the potential is monophasic negative-like and in particular, the electrode recording the highest amplitude (in absolute value) is supposed to be beneath the AIS.

(a)

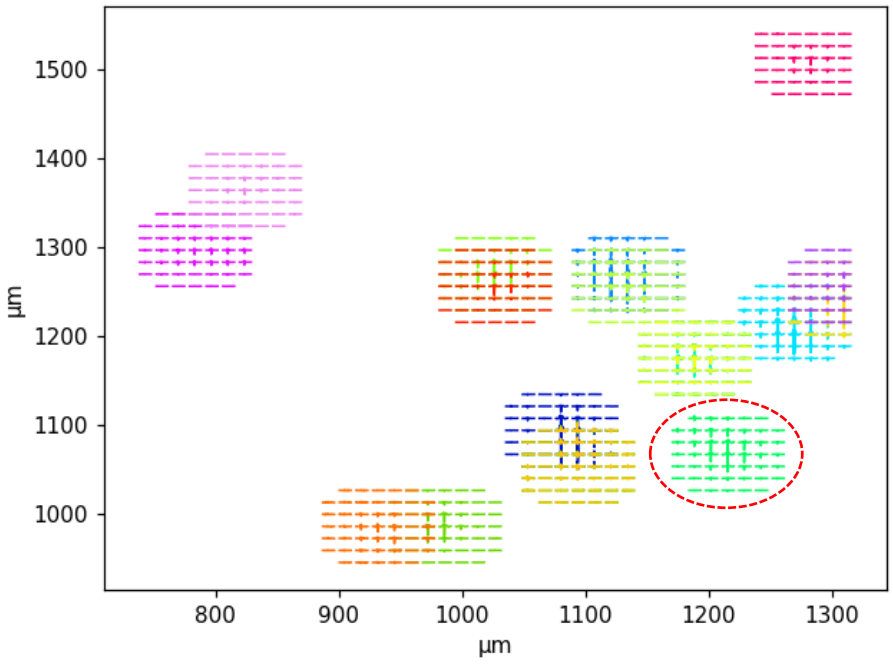

(b)

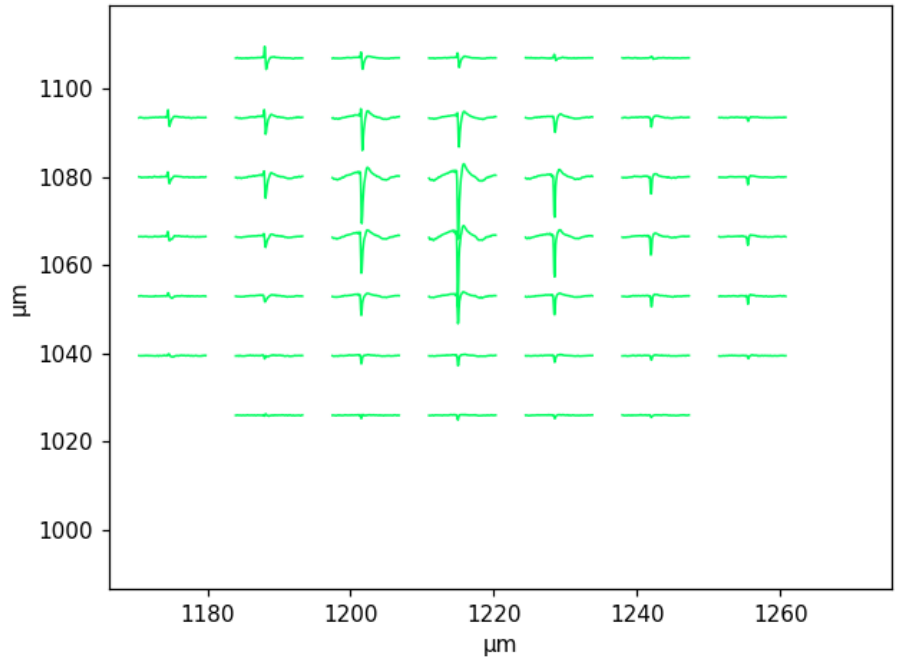

Figure 3.12 Detected neurons at DIV 17. (a) Templates and localization of the neurons on the electrode array region related to the configuration used. The majority of the neurons are situated in the area with the highest peak frequencies. (b) Enlargement of the templates belonging to the neuron in the dashed red line.

When spike sorting is computed, we obtain the spike trains for each neuron. The spike trains are represented using a raster plot. In Figure 3.13a and 3.13b, the raster plot for the detected units is shown at DIV 17.

(a) (b)

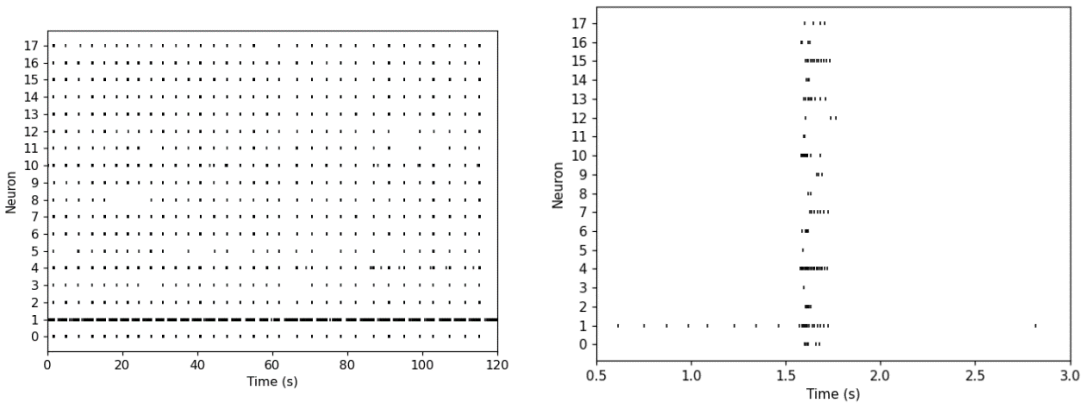

Figure 3.13 Raster plot at DIV 17. (a) Spike trains for each neuron along the whole recording duration. (b) Spike trains in a short window between 0.5 s and 3.0 s.

In this case, 18 neurons are detected by the spike sorter, and they all show burst activity, which means they fire at high frequency in a short time and then remain quiescent, with the phenomenon happening repeatedly. It is possible to notice that there are some neurons like units 1 and 4 oddly more active than the others, if they are neurons or not should be checked by looking at their waveforms (or templates). Alternatively, other tools can be used, like auto-correlogram (ACG) and inter-spike interval. Also, all the other units need to be checked to assess the reliability of the sorter calculation. Looking at the waveforms (Figure 3.14a and 3.14b), the units appear to be real neurons since they resemble the typical shape of extracellular AP.

(a) (b)

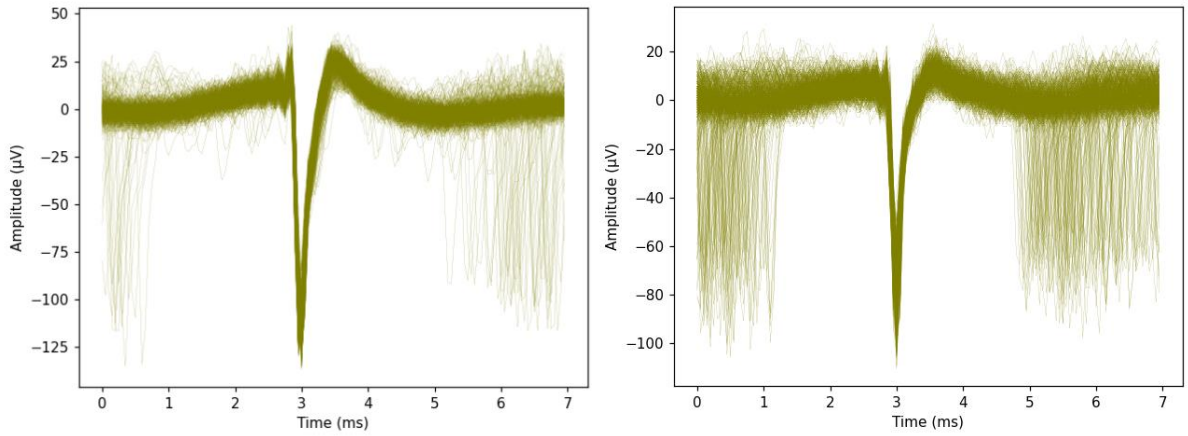

Figure 3.14 Waveforms of two neurons. (a) Unit 1. (b) Unit 4. 140 waveforms having a duration of 7 ms and detected on the highest potential recording channel are overlapped.

The ACGs have the typical shape that has to feature (Figure 3.15), both for units 1 and 4, with a peak at lag 0 ms, since the unit is maximally correlated to itself.

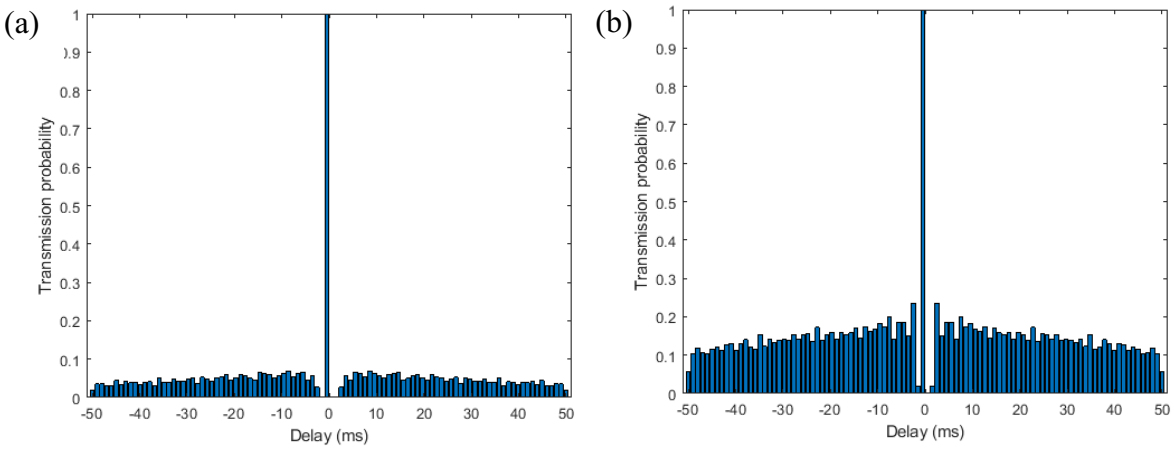

Figure 3.15 Auto-correlogram (ACG) of two neurons. (a) ACG for unit 1. (b) ACG for unit 4. To note the presence of the peak at lag 0 ms: this is what we expect since a neuron must be maximally correlated with itself.

ACG can give a quick idea if the unit is an effective neuron or not. For example, by looking at Figure 3.16, which represents all the ACGs, we can doubt if unit 5 may be a detected cell.

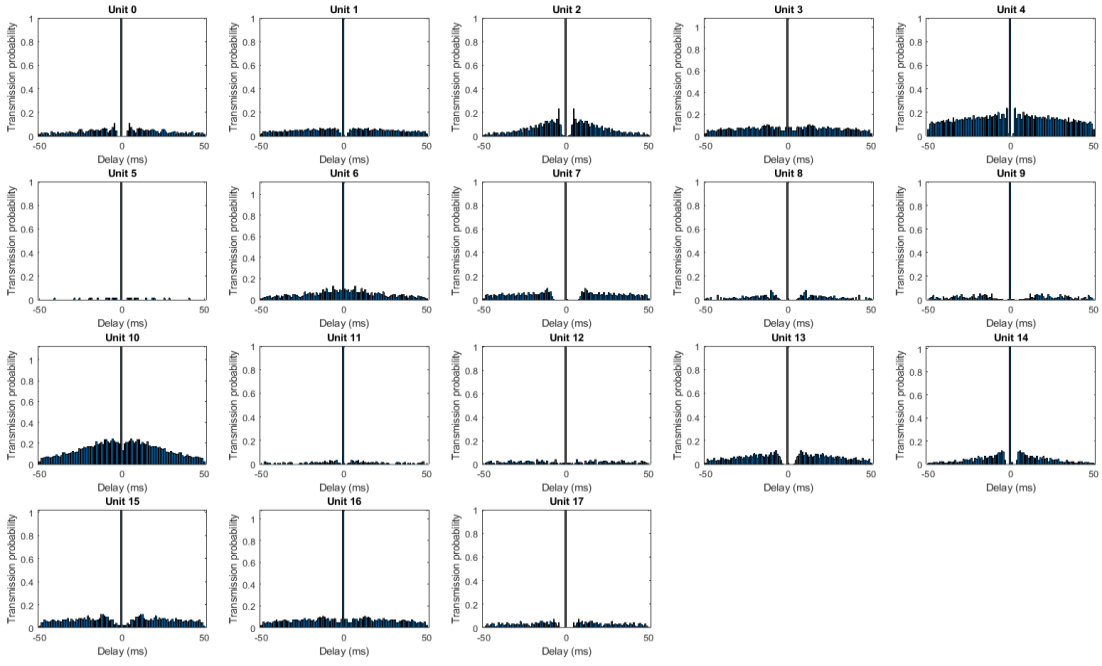

Figure 3.16 ACG of all of the units at DIV 17.

If we plot its waveforms (Figure 3.17a) on the electrode recording the highest potential, the waveforms do not resemble the typical one previously shown. Also, the inter-spike interval distribution (Figure 3.17b) is unrealistic, although no APs violate the refractory period. Having done these considerations, we can confidently mark the unit as a false positive.

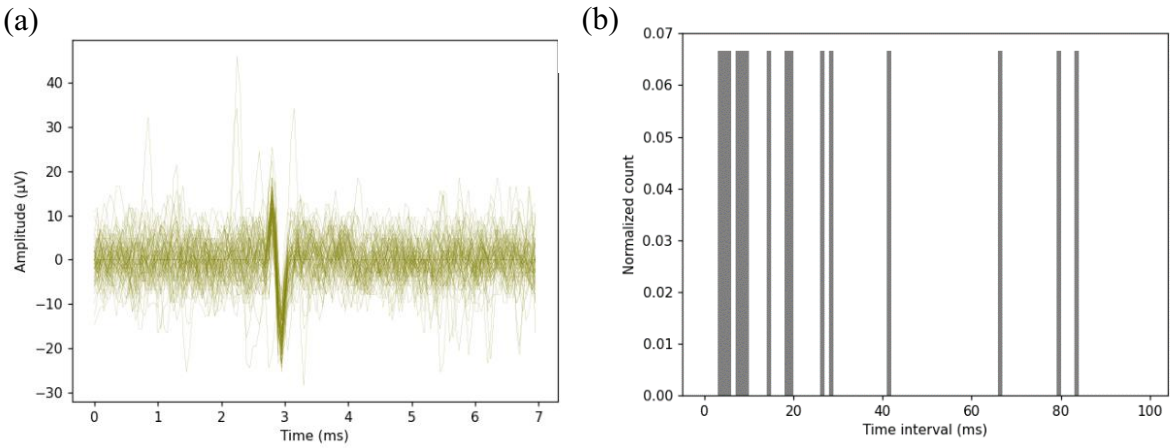

Figure 3.17 False positive neuron. (a) Waveforms. (b) Inter spike interval distribution.

By looking at the raster plot in Figure 3.13a we can think the cells are highly synchronized because they show very similar spiking times. This synchronization should be hypothetically due to the establishment of newborn synaptic connections between the cells. In order to evaluate this potential connection, we can take as an example the CCG of one pair of neurons. The CCG, shown here between unit 7 and unit 13 (Figure 3.18), displays the transmission probability from 7 to 13 and it depicts a peak at a lag of 1-2 ms. Even though not so high, that peak can be explained as a potential connection since the lag is biologically plausible (typically 0.5 – 1 ms is the time delay of the physiological chemical synaptic transmission [55]). When we look at the location of the two units on the chip array (Figure 3.19a) we can clearly see that they are situated pretty near to each other with their templates overlapping. This strengthens the hypothesis of their connection because it would be highly improbable that the two are connected if they are situated too far from each other.

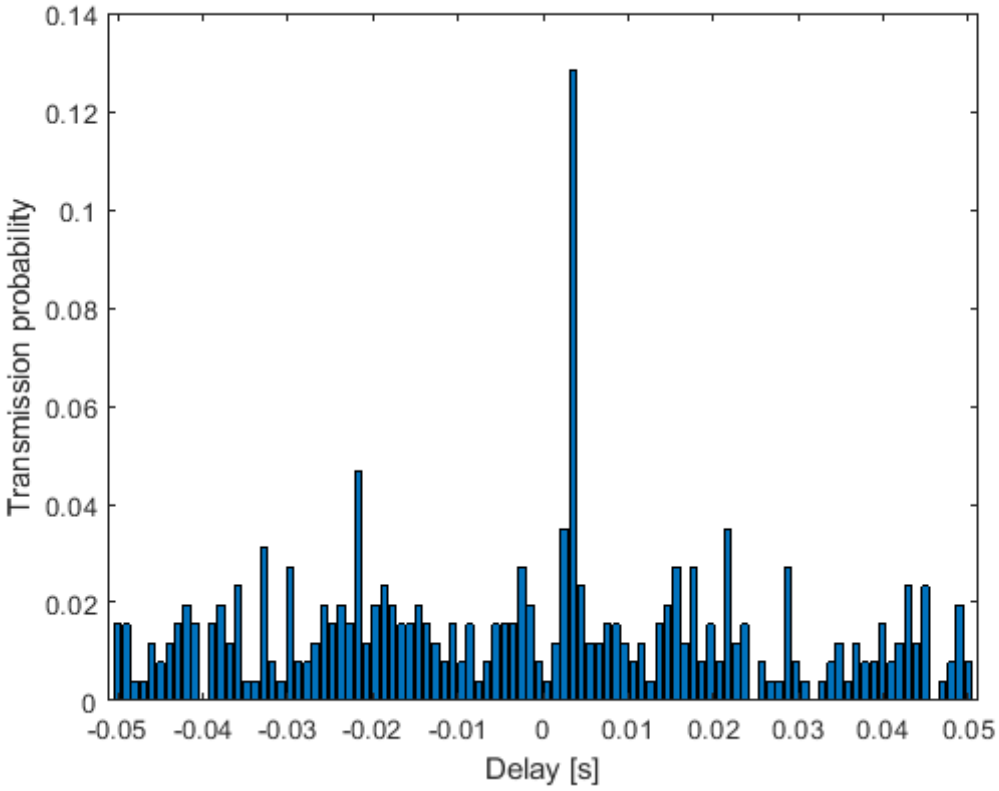

Figure 3.18 Transmission probability between unit 7 and unit 13 at DIV 17.

The recording using the same configuration of electrodes is repeated at DIV 21 to study how the culture evolves. We can see from Figure 3.19a that the majority of neurons that were present at DIV 17 are still detected, but some of them are not present anymore meaning that the sorter was not able to distinguish them or those cells have either died/lost their activity. Also, by checking the raster plot (Figure 3.19b) and comparing it with the one at DIV 17 it seems that all of the cells have experienced a loss of activity.

(a) (b)

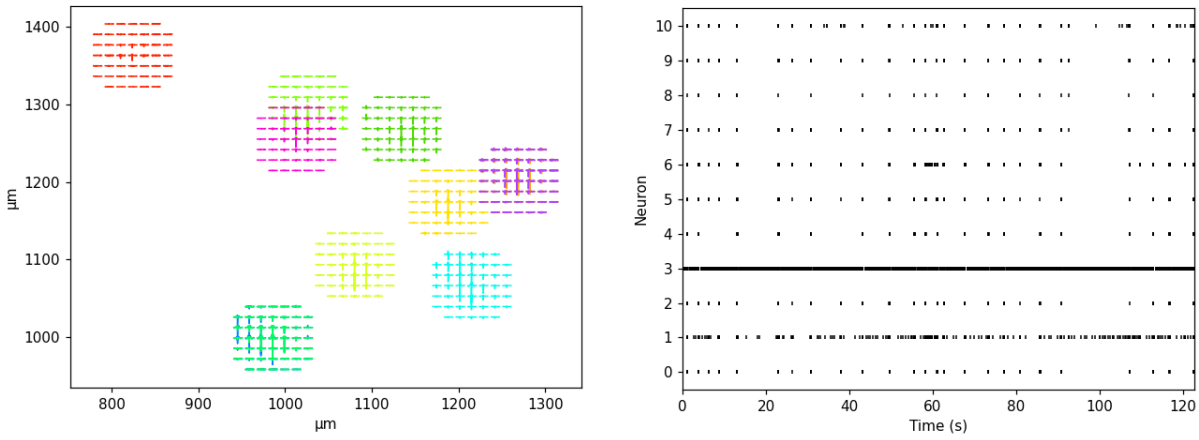

Figure 3.19 Detected neurons at DIV 21. (a) Templates. (b) Raster plot of the spike trains.

What is particularly complex to perform is finding the same neurons in two different recordings. In fact, some neurons can move from their original position or new ones are detected from the spike sorting algorithm. In this case, since the number of neurons is not very high, the presence of unit 7 and unit 13 is manually checked to analyze how the CCG changes. By comparing their locations at DIV 17 and DIV 21 (Figure 3.20a-d), we can confidently state that the neurons are the same: although we cannot state which is unit 7 and which one is unit 13 for sure, due to the template shape similarities it is highly probable that unit 7 is the one in green color while the unit 13 in red and violet.

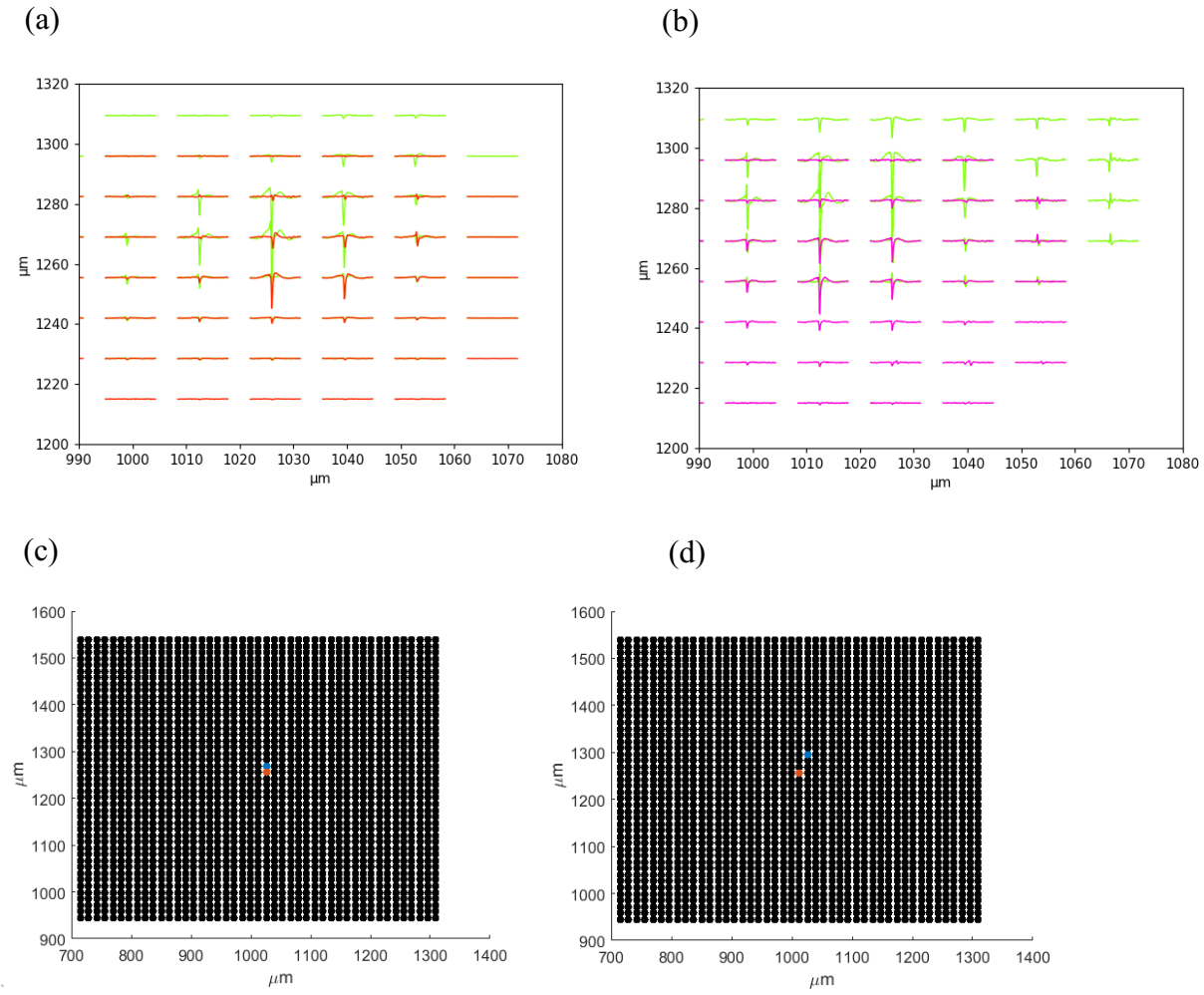

Figure 3.20 Neuron locations. (a) Template locations of units 7 and 13 at DIV 17 and (b) at DIV 21. (c) AIS estimated location at DIV 17 and (d) DIV 24 (unit 7 in red and unit 13 in blue).

We can now look at their CCG (Figure 3.21b) and confront it with the one at DIV 17 (Figure 3.21a): we can notice a lower transmission probability, which could mean a reduction of synaptic connections, or the postsynaptic neuron has become less responsive due to a decrease in its functional activity.

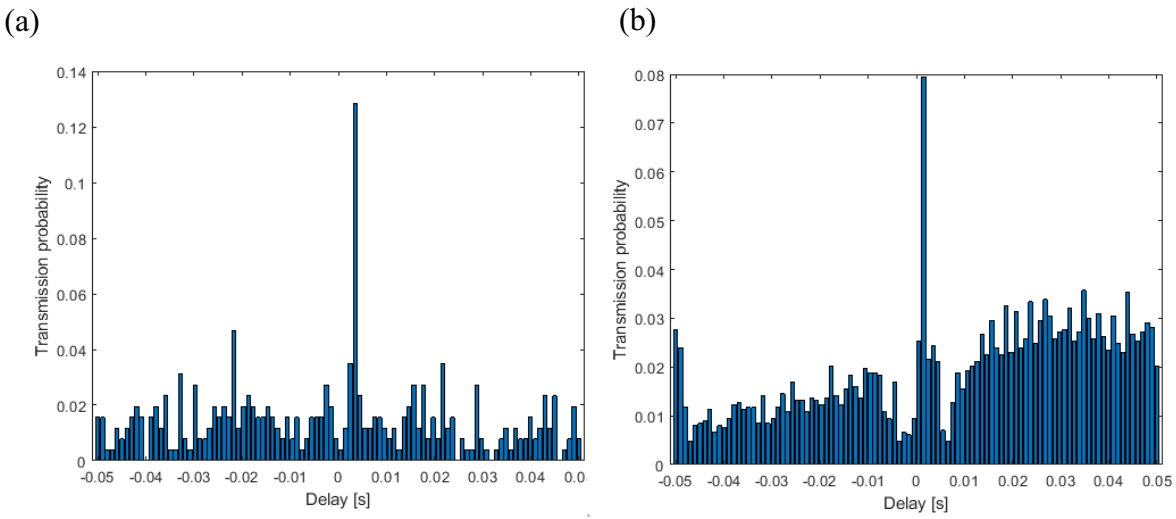

Figure 3.21 Comparison CCG units 7 and 13 at DIV 17 and DIV 21. (a) CCG DIV 17. (b) CCG DIV 21.

The experiments finish here since at DIV 24 spike sorting was not able to detect the presence of any neuron, as we can see from Figure 3.22 showing the raster plot (no unit is found by the sorter).

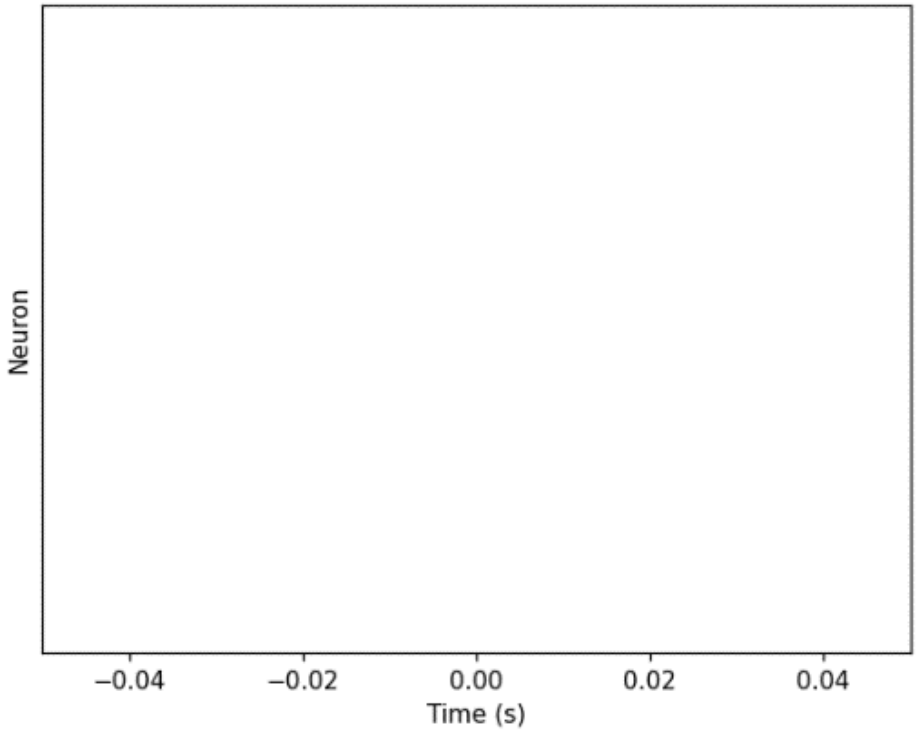

Figure 3.22 Raster plot of the spike trains at DIV 24.

4 Discussion

The original goal of this project was to develop methods to study STDP by applying different stimuli to pairs of neurons. First, various waveforms have been generated in order to assess which one would have been the most effective to evoke AP. A neuron would have been stimulated using the electrode corresponding to the highest potential recorded (presumably beneath the AIS, since it has been demonstrated to be the most sensitive region to the stimulation). After having established the best pulse, a STDP protocol would have been designed by setting a precise pulse frequency and varying the timing between the presynaptic and the postsynaptic stimuli, both of them delivered at the AIS-corresponding electrodes. CCG analysis before and after the stimulation would have been carried out, and ideally, a change should become visible resulting from the short-term plasticity. A peak in the CCG should theoretically show up at the time difference between the two pulses. The CCGs resulting from different neuron pair stimulations would have been compared with a control group, not receiving any stimuli, and statistical analysis would have been performed by considering the changes in the synaptic transmission probability. Also, imaging should have been a tool for validation of the spike sorter's ability to detect neurons and their exact location. In particular, immunostaining with antibodies against MAP-2 (to stain the cytoskeleton) and Ankyrin G (to stain the AIS) would have been performed.

However, different issues should be pointed out to describe the reasons why the aforementioned plan was not successful.

First, the cell culturing protocol as well as the maintenance of the cell culture should be optimized. Although the device can support long-term cultures, the cells are not able to live more than 24 days, which makes it hard to perform experiments after the cells have become functional (typically requiring 14 days from the culture). Even if ideally the cells stayed alive more days, we could just carry out short-term plasticity studies, because long-term plasticity may take weeks or months, which can only be done in vivo at the moment. Short-term plasticity is an effect of the changes in neurotransmitter release at the level of the synaptic cleft, and these are the first changes happening after the cells receive any sort of stimulus (both in vitro, e.g., using electrical stimulation, and in vivo, thanks to experiences,

emotions, and so on). On the other hand, long-term plasticity requires more time to occur, since the changes involve the formation of new synapses or the genesis of new neurons. Being aware of that, more efforts should be spent on establishing an updated protocol that guarantees cell viability during the whole in vitro experiments.

Another reason why cells have not been viable for many days is because of contamination. In addition, methods for assessing the pregnancy of rats must be implemented before sacrificing them, because it can likely happen that rats are not pregnant and we need to wait more time than expected to start new in vitro experiments. This does not affect the results but it can be tedious to experience, unless culturing is done more frequently, in comparison with the actual once in three weeks schedule of the department in which this thesis is carried out. This is necessary if there is the will to realize a new reliable culturing protocol that ensures anyone can perform his experiments.

Looking at the more technical problems, it must be stated that both the hardware and the software need to be severely improved.

Starting with the hardware, during the experiments it can likely happen that the recording unit will suffer from corrosion processes. If corrosion happens, we will not be able to record the signal from the electrodes. Changing the recording unit is not an easy step. If there is not a new recording unit available for substitution, we cannot record any data and this can cause the invalidation of the experiments. Corrosion is most probably due to the humidity inside the incubator. Moreover, the medium can sometimes leak from the device as a result of the formation of breaks or holes in the polycarbonate ring used for enclosing the medium. Leaky devices do not represent just a problem affecting the recording system, but more importantly the cell viability: a leaky chip requires more frequent medium exchange, and if not prematurely assessed, the cell culture inevitably undergoes death.

A phenomenon that every day we need to confront is noise. Noise drastically degrades the quality of the recordings, and a high level of noise can de-facto make it impossible to distinguish AP and therefore detect neurons with the spike sorter. The problem is that sometimes noise can arise from the not sealed connection between the chip and the recording unit, which luckily can be fixed by a simple unplugging-plugging back; other times it can be caused by something difficult to discern and situated in the surrounding environment. That can be sorted out by restarting the entire system. If the issue is not fixed, that could mean that the noise comes from the chip itself, and nothing can be done at this point. The chip must be trashed and the experiment finishes here.

Discussing the software now, the interface the user exploits to interact with the device has to be improved. Quite often, the server is not able to connect with the FPGA that sends the commands to the device. It may require some time because we would just need to try reconnecting to fix this problem. A major problem is that the data stream, which is properly working for a while, suddenly stops, meaning that no signal can be recorded. The only way to solve this is to restart the system. If it occurs while doing a signal recording, a new one should be started.

Some interface commands do not respond sometimes, as when you have to save a recording file. Consequently, it forces the user to stop the recording manually using the terminal command window, through a complex process that inevitably requires some time. The occurrence of this event is quite random, so there is no way to avoid this.

Another command which is not properly working is the stimulation interface: even if everything is correctly set up, the electrodes might not be able to release the stimulus, maybe because of an error in the server.

In the end, random freezes of the whole software happen. In light of these issues, it is evident that the interface should be updated or a new one to be developed if the user wants to work "sheltered", otherwise, it would become unpleasant working with such errors, especially when they start to appear too frequently.

Moving to the results, it has to be told that the number of detected neurons is strictly dependent upon the length of the recording, with longer recordings showing better results than shorter ones. A longer recording can capture neurons firing at low frequencies, and it allows us to understand how the cells are behaving during long time periods. However, spike sorting performed on a longer recording unavoidably takes a longer time to complete, where the feature extraction and clustering are the main "heavy" processes. Actually, the recording length does not directly affect the spike sorting computational time, but it is the total number of spikes the sorter needs to distinguish and cluster. Generally, however, longer recordings entail a longer computational time. Also, a larger number of electrodes means a larger volume of data. A compromise should be found to ensure the detection of neurons; in this thesis, 120 s is the length of the recording chosen, since it has been seen that several hours are needed using a longer duration (up to days).

One of the main spike sorting problems is the presence of overlapping spikes, especially when we have a few recording electrodes. Using more electrodes recording in the same area reduces the probability of this event because, if two neurons may appear similar to

each other in one electrode, they will not in others since they are situated at a different distance from the recording electrodes. Of course, as previously said, the disadvantage is a larger size of data to be processed.

As we saw from the results, two types of phenomena are happening when applying a stimulus, which should not occur: first, the amplifier saturation when setting 20 mV or 30 mV with a gain of 32 (recalling that the voltage operational range is 2 V), and secondly, the presence of an opposite waveform after the pulse which induces amplifier saturation as well from a certain voltage amplitude. These events may have different explanations. Regarding the first problem, it must be stated that the system is not suitable for delivering small voltages (tens of millivolts) because the DAC has a 3 mV-resolution, therefore the stimulation cannot be precise. Instead, hundreds of millivolts can be precisely delivered, but this is not a problem since AP can be evoked with hundreds of millivolts amplitude. Moreover, the gain may not be actually the one set, so this factor combined with the low resolution of the DAC may end up with clipping even at 20 mV. For what concerns the second problem, since we saw it does not happen when the system is disconnected from the amplifiers, we hypothesize that the opposite waveform can be a result of charge accumulation processes at the double layer capacitance of the electrode, that is given back after the stimulation pulse is finished. Along with that, the stimulation buffer may not able to remove all of the charges after the stimulus, thus the opposite waveform.

Regarding the electrophysiological characterization, we noticed that rat cortical neurons need at least 14 DIV to start measuring their activity.

Spike sorting is a heavy process, ideally one would want to perform the sorting on all the MEA to find all neurons. Here, only a small region of the chip has been targeted for spike sorting, because repeating the same process many times would have also required too much time.

Spike sorting, as it has been shown, is not always accurate and some units can represent false positives due to misclassification errors, mainly provoked by noise and the presence of overlapping spikes. Noise is the main source of errors: ensuring a low noise level can minimize the misclassifications since the amplitude distribution of each spike and that one of the noise will be separated enough. Fortunately, most of the time we can recognize the errors thanks to the analysis of the waveforms, inter-spike interval, and ACG. Of course, different spike sorters do exist, and it is possible to measure the performance of each sorter and compare them to each other in order to establish which one is the best.

The raster plot results have shown neurons' tendency to synchronize their activity when they are spontaneously firing. This is expected since at the postnatal stage of development neurons are capable of forming small networks generating repeated and organized spike patterns, with electrical synapses gradually switching to chemical synapses.

CCG analysis is a powerful tool that allows estimating potentially connected neurons. CCG also enables us to study how these connections evolve over time. However, a big issue is finding the same neurons in different recordings: doing so manually can be highly time-consuming if there are too many units for similarity checking; in that case, automatic tools have to be implemented, e.g., measuring the cosine distance between the footprints. In addition, we are not able to confirm if there is a synaptic connection or not; the only way to validate the results is by the use of microscopy.

Another big issue is the impossibility to perform the spike sorting online. In fact, we need to save all of the spikes before doing the spike sorting, and this inevitably makes all the processes be operated offline. Online spike detection can be a fascinating field but, at the moment, the majority of the sorters work offline because clustering can be performed only after having stored all the spike trains. Online spike sorting would be implemented in closed-loop experiments and it will be essential for developing brain-machine interfaces. To achieve this goal, still, a lot of research has to be carried out.

Finally, implementing new biological sensors for common parameters, like pH, O_2, temperature, and other more specific, e.g., electrolyte concentrations such as Ca^{2+}, would also allow a more comprehensive understanding of the actual state of the cells.

5 Conclusion

In this thesis, electrochemical characterization of neural cultures was performed by using a newly developed HD-MEA featuring 59 760 microelectrodes. The device was first packaged and Pt-black was electrodeposited on the electrodes to reduce the noise. Next, a spike sorting algorithm was chosen to locate the neurons in a specific area of the array. The detected neurons were manually checked to distinguish if they are true or false positives. As we saw, the number of detected neurons is not so high but, generally, the units seemed to be effective neurons. This cannot be told for sure, since only staining would be able to verify these results. Next, CCG analysis was used to find putative pairs of connected neurons for STDP stimulation. Different pulses were designed and delivered in PBS to study the accuracy of the stimulation unit. It was noticed that the system was not capable to deliver low amplitude voltage pulses, because of the DAC resolution. In addition, amplifier saturation occurred at below threshold voltage due to the not precise gain settings. Also, after the pulse an opposite waveform appears, which can be attributed to charge accumulation at the level of the electrodes. Stimulation at the AIS of the respective neuron should have been the next step but was not carried out because of hardware and biological issues.

This is why research has to focus on the development of a reliable cell culturing protocol that guarantees high cell viability. Spike sorting has to be improved to manage longer recordings, and most of all new spike sorting algorithms should be generated to work online if the goal is to realize brain-human interfaces. Once these problems have been solved, then it would be possible to exploit all the potential this device has, and achieve insights into how neural cells interact with each other and how they react in response to external stimulation.

Bibliography

[1] D. U. Silverthorn, *Fisiologia umana*, 1st ed. Città di Castello: Pearson, 2017.

[2] R. Splittgerber and R. S. Snell, *SNELL'S CLINICAL NEUROANATOMY*, 8th ed. Philadelphia: Wolters Kluwer, 2019.

[3] D. Krishnagopal, *The Biology of Thought*, 1st ed. Cambridge: Academic Press, 2014.

[4] J. Moini, N. G. Avgeropoulos, and M. Samsam, "Cytology of the nervous system", in *Epidemiology of Brain and Spinal Tumors*, pp. 41–63, 2021, doi: 10.1016/b978-0-12-821736-8.00012-1.

[5] C. Y. M. Huang and M. N. Rasband, "Axon initial segments: structure, function, and disease", *Annals of the New York Academy of Sciences*, vol. 1420, pp. 46–61, 2018. doi: 10.1111/nyas.13718.

[6] J. A. White, "Action Potential", in *Encyclopedia of the Human Brain*, vol. 1, pp. 1–12, 2002. doi:10.1016/B0-12-227210-2/00004-2.

[7] D. U. Silverthorn, *Human Physiology: An Integrated Approach,* 5th ed. USA: Pearson, 2010.

[8] Purves D and Augustine GJ, *Neuroscience*, 2nd ed. Sunderland: Sinauer Associates, 2001.

[9] B. W. Connors and M. A. Long, "Electrical synapses in the mammalian brain", *Annual Review of Neuroscience*, vol. 27. pp. 393–418, 2004. doi: 10.1146/annurev.neuro.26.041002.131128.

[10] F. Gabbiani and S. J. Cox, *Mathematics for neuroscientists*, 1st ed. Amsterdam ; Boston: Elsevier Academic Press, 2010.

[11] T. C. Südhof, "The presynaptic active zone", *Neuron*, vol. 75, pp. 11–25, 2012. doi: 10.1016/j.neuron.2012.06.012.

[12] M. Yoshihara and J. T. Littleton, “Synaptotagmin I Functions as a Calcium Sensorto Synchronize Neurotransmitter Release”, *Neuron*, vol. 36, pp. 897–908, 2002. doi: 10.1016/s0896-6273(02)01065-6.

[13] N. A. Ramakrishnan, M. J. Drescher, and D. G. Drescher, “The SNARE complex in neuronal and sensory cells”, *Molecular and Cellular Neuroscience*, vol. 50, pp. 58–69, 2012. doi: 10.1016/j.mcn.2012.03.009.

[14] G. L. Fain and T. J. O’Dell, *Molecular and Cellular Physiology of Neurons*, 2nd ed. Cambridge: Harvard University Press, 2014.

[15] T. L. Schwarz, “Synaptotagmin promotes both vesicle fusion and recycling”, vol. 101, pp. 16401 – 16402, 2004. doi:1073pnas.0407390101.

[16] J. H. Byrne, “Postsynaptic Potentials and Synaptic Integration”, in *From Molecules to Networks: An Introduction to Cellular and Molecular Neuroscience: Third Edition*, pp. 489–507, 2014. doi: 10.1016/B978-0-12-397179-1.00016-6.

[17] A. J. Barker and E. M. Ullian, “Astrocytes and synaptic plasticity”, *Neuroscientist*, vol. 16, pp. 40–50, 2010. doi: 10.1177/1073858409339215.

[18] J. R. Hughes, “Post-Tetanic Potentiation”, *American Physiology Society-Physiological Reviews*, vol. 38, pp. 91–113, 1958. doi:10.1152/physrev.1958.38.1.91.

[19] T. V. P. Bliss and T. Lomo, “Long-lasting potentiation of synaptic transmission in the dentate area of the anaesthetized rabbit following stimulation of the perforant path”, *The Journal of Physiology*, vol. 232, pp. 331–356, 1973. doi: 10.1113/jphysiol.1973.sp010273.

[20] L. Hao, Z. Yang, and J. Lei, “Underlying mechanisms of cooperativity, input specificity, and associativity of long-term potentiation through a positive feedback of local protein synthesis”, *Frontiers in Computational Neuroscience*, vol. 12, [no pagination], 2018, doi: 10.3389/fncom.2018.00025.

[21] R. C. Malenka, “The long-term potential of LTP”, *Nature*, vol. 4, pp. 923–926, 2003. doi: 10.1038/nrn1258.

[22] T. Sumi and K. Harada, “Mechanism underlying hippocampal long-term potentiation and depression based on competition between endocytosis and

exocytosis of AMPA receptors", *Scientific Reports*, vol. 10, [no pagination], 2020, doi: 10.1038/s41598-020-71528-3.

[23] M. A. Lynch, "Long-Term Potentiation and Memory", *American Physiology Society-Physiological Reviews*, vol. 84, pp. 87–136, 2004, doi: 10.1152/physrev.00014.2003.

[24] J. R. Sanes and J. W. Lichtman, "Can molecules explain long-term potentiation?", *Nature Neuroscience*, vol. 2, pp. 597–604, 1999. doi:10.1038/10154.

[25] S. B. Baltaci, R. Mogulkoc, and A. K. Baltaci, "Molecular Mechanisms of Early and Late LTP", *Neurochemical Research*, vol. 44, pp. 281–296, 2019. doi: 10.1007/s11064-018-2695-4.

[26] R. C. Malenka, "Synaptic Plasticity in the Hippocampus: LTP and LTD", *Cell*, vol. 76, pp. 535–536, 1994. doi: 10.1016/0092-8674(94)90517-7.

[27] J. Lisman, "A mechanism for the Hebb and the anti-Hebb processes underlying learning and memory (calmodulin/calcium/calmodulin-dependent protein kinase II/protein phosphatase 1/adenylate cyclase/calcineurin)", *Neurobiology*, vol. 86, pp. 9574 – 9578, 1989. doi: 10.1073/pnas.86.23.9574.

[28] Q. Zhou, K. J. Homma, and M. M. Poo, "Shrinkage of dendritic spines associated with long-term depression of hippocampal synapses", *Neuron*, vol. 44, pp. 749–757, 2004. doi: 10.1016/j.neuron.2004.11.011.

[29] G. L. Collingridge, S. Peineau, J. G. Howland, and Y. T. Wang, "Long-term depression in the CNS", *Nature Reviews Neuroscience*, vol. 11, pp. 459–473, 2010. doi: 10.1038/nrn2867.

[30] S. Insuk and L. H. Richard, "Regulation of AMPA receptors during synaptic plasticity", *Cell*, vol. 25, pp. 578–588, 2002. doi: 10.1016/s0166-2236(02)02270-1.

[31] D. O. Hebb, *The Organisation of Behaviour*. New York: John Wiley & Sons, 1949.

[32] J. J. Langille and R. E. Brown, "The synaptic theory of memory: A historical survey and reconciliation of recent opposition", *Frontiers in Systems Neuroscience*, vol. 12, [no pagination], 2018, doi: 10.3389/fnsys.2018.00052.

[33] T. B. Christophel, P. C. Klink, B. Spitzer, P. R. Roelfsema, and J. D. Haynes, "The Distributed Nature of Working Memory", *Trends in Cognitive Sciences*, vol. 21, pp. 111–124, 2017. doi: 10.1016/j.tics.2016.12.007.

[34] E. B. O'Neil *et al.*, "Distinct patterns of functional and effective connectivity between perirhinal cortex and other cortical regions in recognition memory and perceptual discrimination", *Cerebral Cortex*, vol. 22, pp. 74–85, 2012, doi: 10.1093/cercor/bhr075.

[35] R. M. Mulkey and R. C. Malenka, "Mechanisms Underlying Induction of Homosynaptic Long-Term Depression in Area CA1 of the Hippocampus", *Neuron*, vol. 9, pp. 967–975, 1992. doi: 10.1016/0896-6273(92)90248-c.

[36] S. M. Dudek and M. F. Bear, "Homosynaptic long-term depression in area CAl of hippocampus and effects of N-methyl-D-aspartate receptor blockade (long-term potentiation/hippocampal slice/synaptic plasticity/learning/memory)", *Neurobiology*, vol. 89, pp. 4363–4367, 1992. doi: 10.1073/pnas.89.10.4363.

[37] G. M. Wittenberg and S. S. H. Wang, "Malleability of spike-timing-dependent plasticity at the CA3-CA1 synapse", *Journal of Neuroscience*, vol. 26, pp. 6610–6617, 2006, doi: 10.1523/JNEUROSCI.5388-05.2006.

[38] W. B. Levy, "Temporal contiguity requirements for long-term associative potentiation/depression in the hippocampus", *Neuroscience*, vol. 8, pp. 791 – 797, 1983. doi:10.1016/0306-4522(83)90010-6.

[39] H. Markram, W. Gerstner, and P. J. Sjöström, "A history of spike-timing-dependent plasticity", *Frontiers in Synaptic Neuroscience*, pp. 1–24, 2011. doi: 10.3389/fnsyn.2011.00004.

[40] G.-Q. Bi and M.-M. Poo, "Synaptic Modifications in Cultured Hippocampal Neurons: Dependence on Spike Timing, Synaptic Strength, and Postsynaptic Cell Type", *The Journal of Neuroscience,* vol. 18, pp. 10464 – 10472, 1998. doi:10.1523/JNEUROSCI.18-24-10464.1998

[41] D. E. Feldman, "Timing-Based LTP and LTD at Vertical Inputs to Layer II/III Pyramidal Cells in Rat Barrel Cortex", *Neuron*, vol. 27, pp. 45–56, 2000. doi: 10.1016/s0896-6273(00)00008-8.

[42] R. C. Froemke and Y. Dan, “Spike-timing-dependent synaptic modification induced by natural spike trains”, *Nature*, vol. 416, pp. 433–438, 2002. doi: 10.1038/416433a.

[43] P. Safo and W. G. Regehr, “Timing dependence of the induction of cerebellar LTD”, *Neuropharmacology*, vol. 54, pp. 213–218, 2008, doi: 10.1016/j.neuropharm.2007.05.029.

[44] N. Caporale and Y. Dan, “Spike timing-dependent plasticity: A Hebbian learning rule”, *Annual Review of Neuroscience*, vol. 31. pp. 25–46, 2008. doi: 10.1146/annurev.neuro.31.060407.125639.

[45] A. Hierlemann, U. Frey, S. Hafizovic, and F. Heer, “Growing cells atop microelectronic chips: Interfacing electrogenic cells in vitro with CMOS-based microelectrode arrays”, *Proceedings of the IEEE*, vol. 99, pp. 252–284, 2011, doi: 10.1109/JPROC.2010.2066532.

[46] J. M. Goaillard, E. Moubarak, M. Tapia, and F. Tell, “Diversity of Axonal and Dendritic Contributions to Neuronal Output”, *Frontiers in Cellular Neuroscience*, vol. 13, [no pagination], 2020. doi: 10.3389/fncel.2019.00570.

[47] M. E. J. Obien, K. Deligkaris, T. Bullmann, D. J. Bakkum, and U. Frey, “Revealing neuronal function through microelectrode array recordings,” *Frontiers in Neuroscience*, vol. 9, p. 423, 2015. doi: 10.3389/fnins.2014.00423.

[48] F. Franke *et al.*, “High-density microelectrode array recordings and real-time spike sorting for closed-loop experiments: An emerging technology to study neural plasticity”, *Frontiers in Neural Circuits*, vol. 6, [no pagination], 2012. doi: 10.3389/fncir.2012.00105.

[49] S. Ronchi *et al.*, “Single-Cell Electrical Stimulation Using CMOS-Based High-Density Microelectrode Arrays”, *Frontiers in Neuroscience*, vol. 13, 2019, doi: 10.3389/fnins.2019.00208.

[50] D. J. Bakkum *et al.*, “The Axon Initial Segment is the Dominant Contributor to the Neuron’s Extracellular Electrical Potential Landscape”, *Advanced Biosystems*, vol. 3, 2019, doi: 10.1002/adbi.201800308.

[51] J. Dragas *et al.*, “In Vitro Multi-Functional Microelectrode Array Featuring 59 760 Electrodes, 2048 Electrophysiology Channels, Stimulation, Impedance Measurement, and Neurotransmitter Detection Channels”, *IEEE J Solid-State Circuits*, vol. 52, pp. 1576–1590, 2017, doi: 10.1109/JSSC.2017.2686580.

[52] V. Viswam, “High-Density Multi-Functional Neural Interface in CMOS Technology”, ETH Zurich, Basel, Switzerland, 2016.

[53] S. Garcia and C. Pouzat, “Welcome to tridesclous’s documentation!”, https://tridesclous.readthedocs.io/en/latest/ (accessed Apr. 14, 2022).

[54] A. P. Buccino and S. Garcia, “Welcome to SpikeInterface’s documentation!” https://spikeinterface.readthedocs.io/ (accessed Apr. 14, 2022).

[55] M. Caire, V. Reddy, and M. Varacallo, “Physiology, Synapse”, https://www.ncbi.nlm.nih.gov/books/NBK526047/ (accessed Apr. 14, 2022).

[56] B. Raziyeh, V. Viswam, “Electrical Impedance Tomography on Highdensity Microelectrode Arrays”, https://ethz.ch/content/dam/ethz/special-interest/bsse/bioengineering/pdfs/MT_NeuroCMOS%20EIT.pdf (accessed Aug 1, 2022).

[57] K. Kirkland, “Crosscorrelation” https://www.med.upenn.edu/mulab/crosscorrelation.html (accessed May 25, 2022).

Appendix A

A.1 Device and hardware setup

In this thesis, a newly developed 0.18-µm CMOS HD-MEA is exploited, which comprises 59 760 Pt planar electrodes, arranged in a 332 x 180 layout with a covered area of 4.48 x 2.43 mm^2. The inter-electrode distance is 13.5 µm, with each electrode having a size of 3.0 x 7.5 $µm^2$ (Figure A.1). The system includes 2048 AP recording units, 32 LFP units, 32 impedance measurement units, 28 neurotransmitter detection units, 32 current recording units, and 16 voltage/current stimulation units. The electrodes are fabricated on a silicon wafer. Via plasma-enhanced chemical vapor deposition, a SiO_2/Si_3N_4 passivation stack is deposited to prevent the release of toxic elements (aluminum and copper) in the medium solution as well as to protect the chip from corrosion due to the presence of salts in the medium. The chip is wire-bonded to a printed circuit board (PCB) as it arrives at the user. The electronic characteristics of the device are not going to be discussed here, since they do not represent the purpose of the thesis. For a detailed description of each compartment and its electronic components, the reader is referred to [51]. In the materials and methods section, post-processing is described.

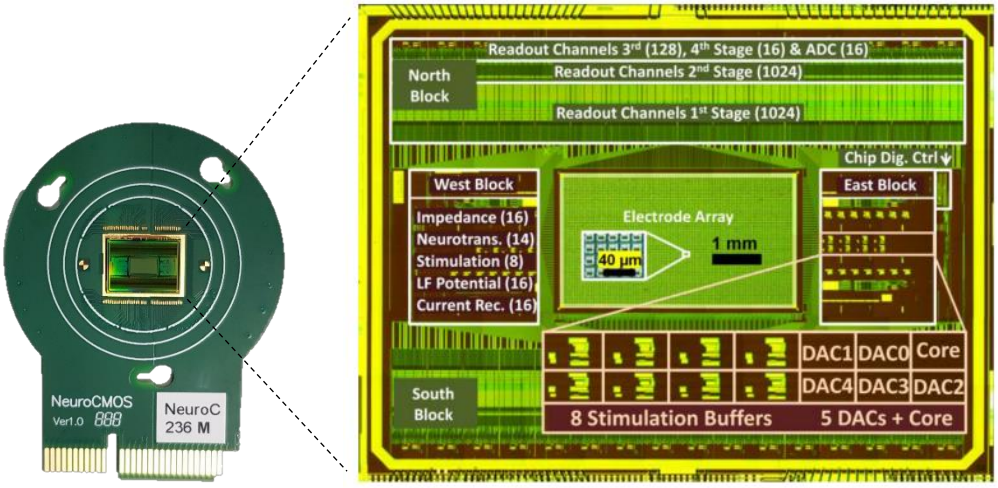

Figure A.1 The 59 760 electrodes HD-MEA. (a) PCB 59 760-electrodes HD-MEA. (b) Photomicrograph of HD-MEA chip [56].

Among the aforementioned functional units, AP recording and stimulation are the ones employed during the experiments.

The user can arbitrarily choose any subset of 2048 AP recording units thanks to switch-matrix circuitry. The recorded signal can be amplified with a programmable gain from 29 dB to 77 dB, in steps of 6 dB. The channels feature a 5.4 μV_{RMS} noise in the band 1 Hz - 10 kHz.

Regarding stimulation, the system is provided with 16 stimulation buffers divided into two blocks (East and West) and 5 DACs to generate the stimulation waveforms.

The data is sampled at 20 kHz, digitized by a 10-bit analog-to-digital converter (ADC), and sent to a field-programmable gate array (FPGA) (Xilinx Zinq, San Jose, USA). The FPGA contains the programmable logic necessary to direct the commands coming from a host computer to the chip at 48 MHz with a high temporal resolution. The output data is acquired using a NI PXIe-6544 high-speed data acquisition card (DAQ) (National Instruments, Austin, USA) card and streamed to a host computer. A scheme of the setup can be visualized in Figure A.2.

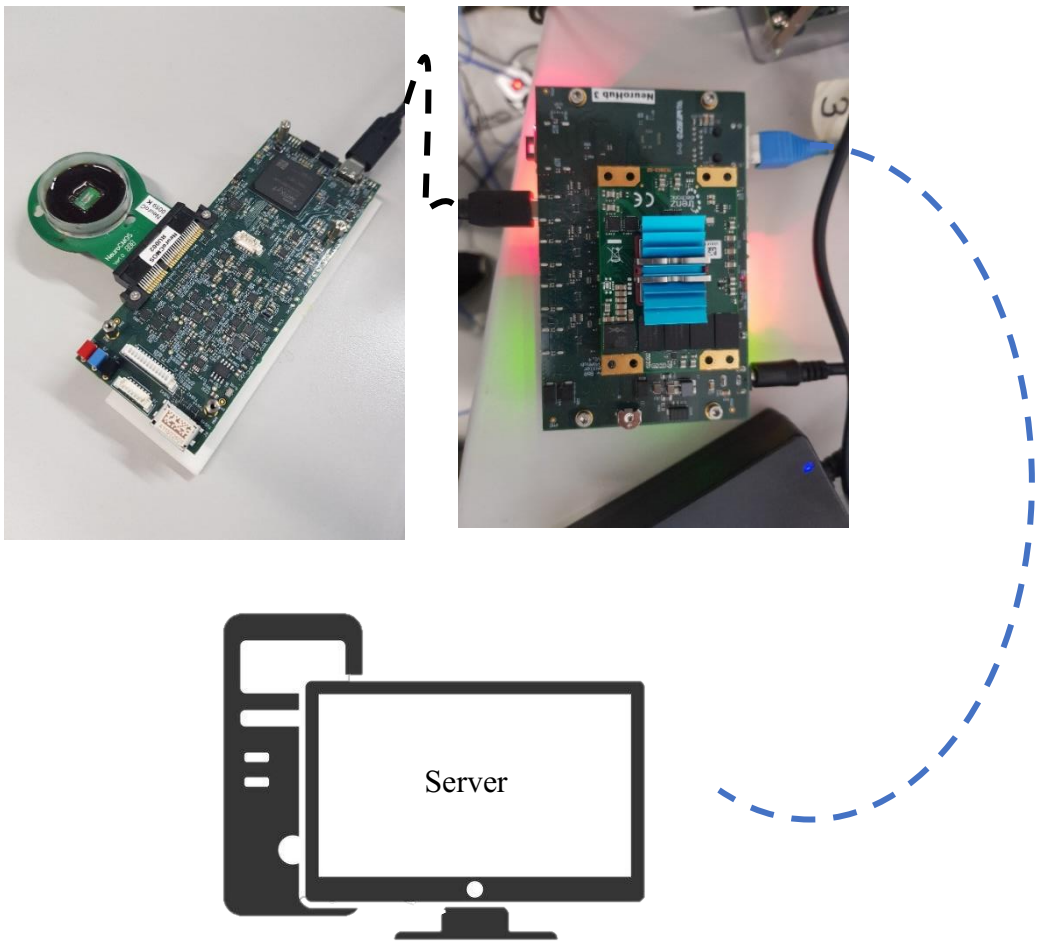

Figure A.2 Setup. On the top-left corner, there is the recording unit with packaged chip plugged in (which can be accommodated into an incubator), on the right corner there is the FPGA, and at the bottom there is the host computer for sending commands. The black dashed line represents the USB-C connection while Ethernet/USB3 connection is indicated with the blue one.

A.2 Graphical User Interface

To interact with the FPGA, a custom-made software is used. The main windows are depicted here, along with the major commands.

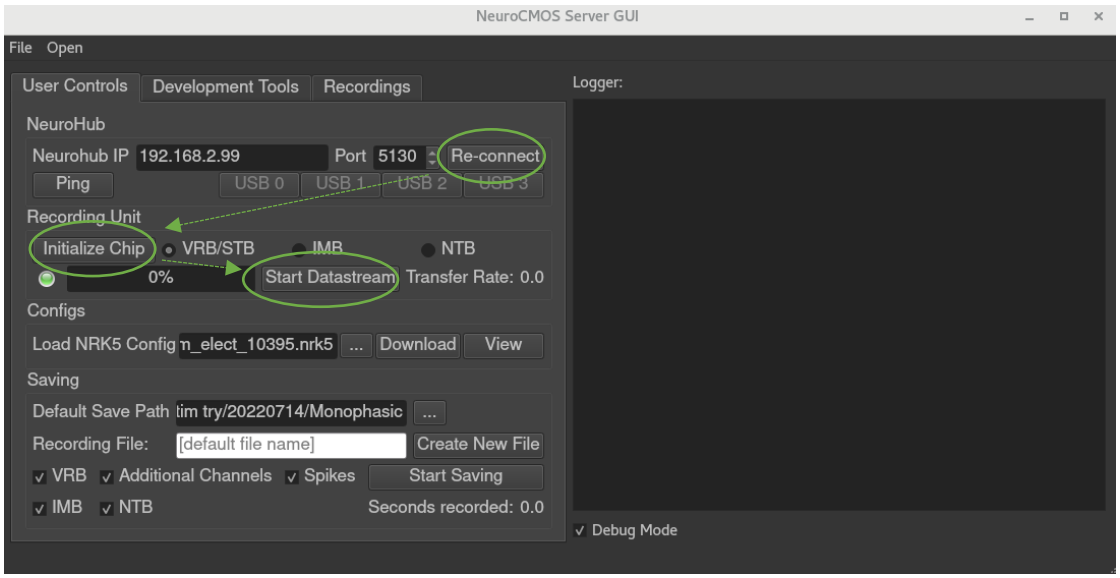

Figure A.3 Chip initialization. 1) Connection 2) Initialization 3) Starting datastream.

An electrode map configuration for stimulation should be chosen among the available ones or it has to be generated.

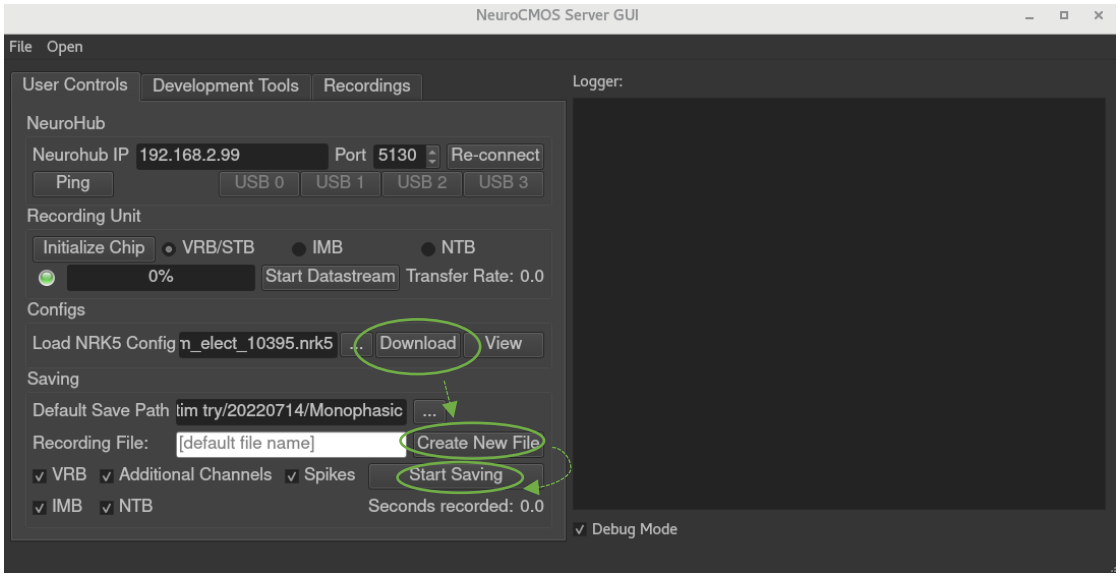

Figure A.4 Recording. 1) Download electrode configuration 2) Create file 3) Save.

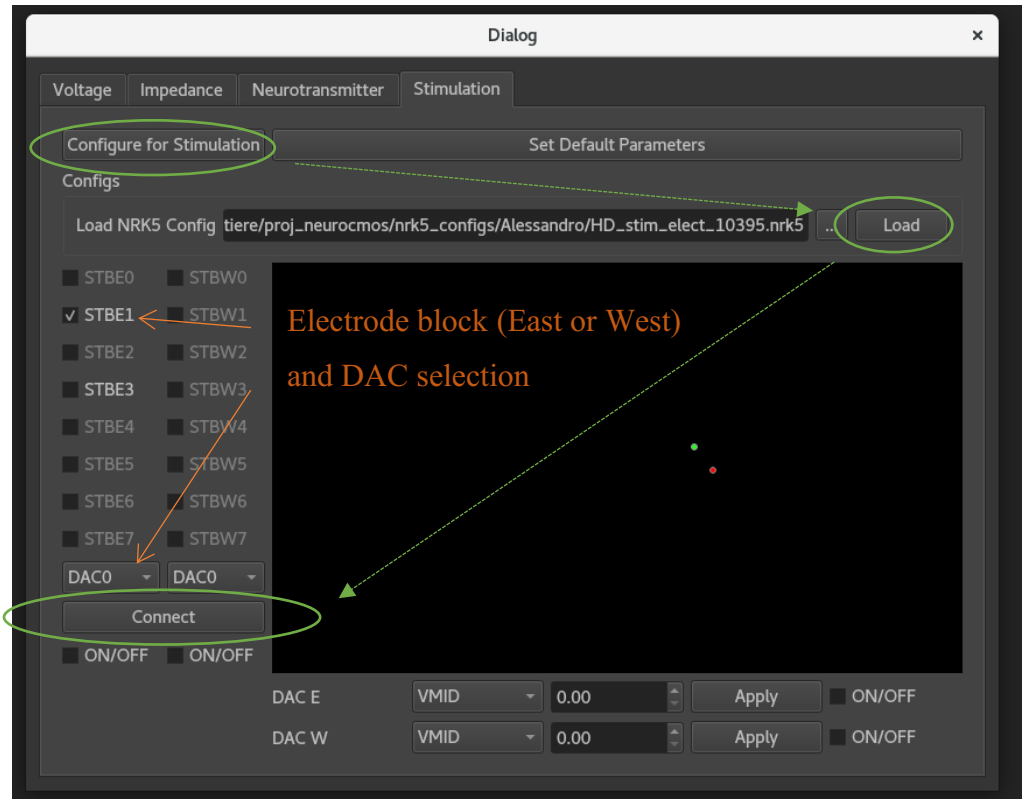

Figure A.5 Connection of the stimulation electrodes. 1) Configure the chip for stimulation 2) Load the electrode configuration 3) Select the electrode block and DAC 4) Connection.

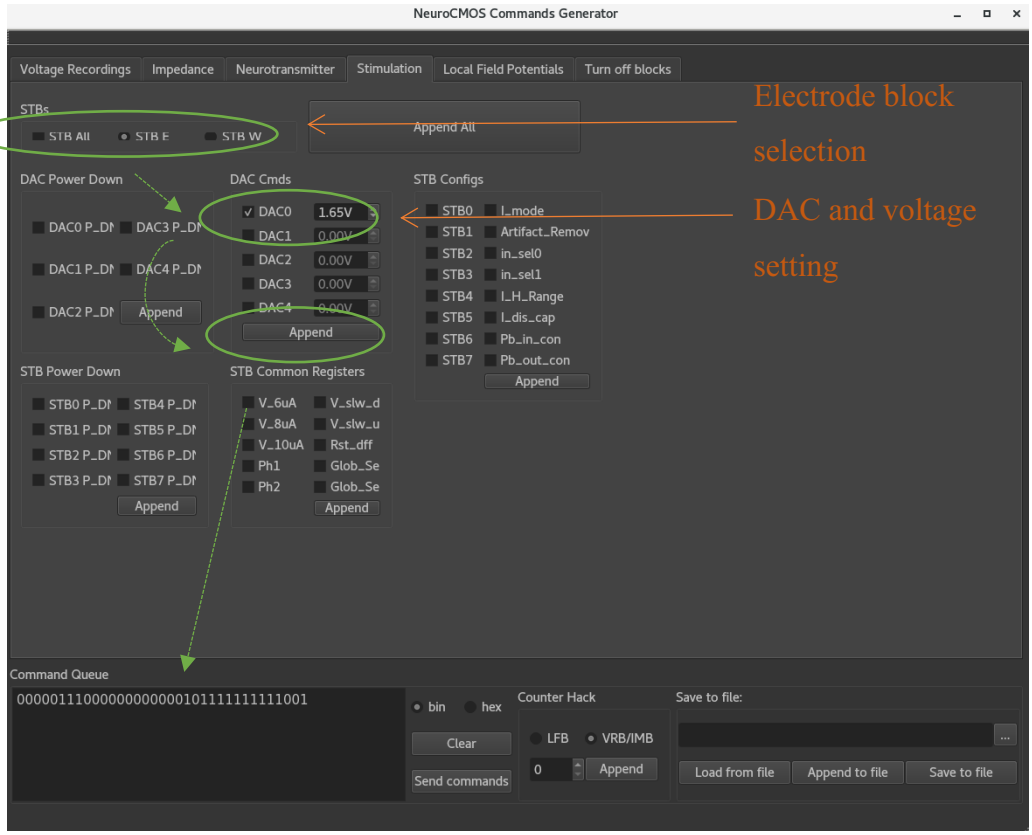

Figure A.6 Pulse design. 1) Select the electrode block 2) Select the DAC and set voltage 3) Append command.

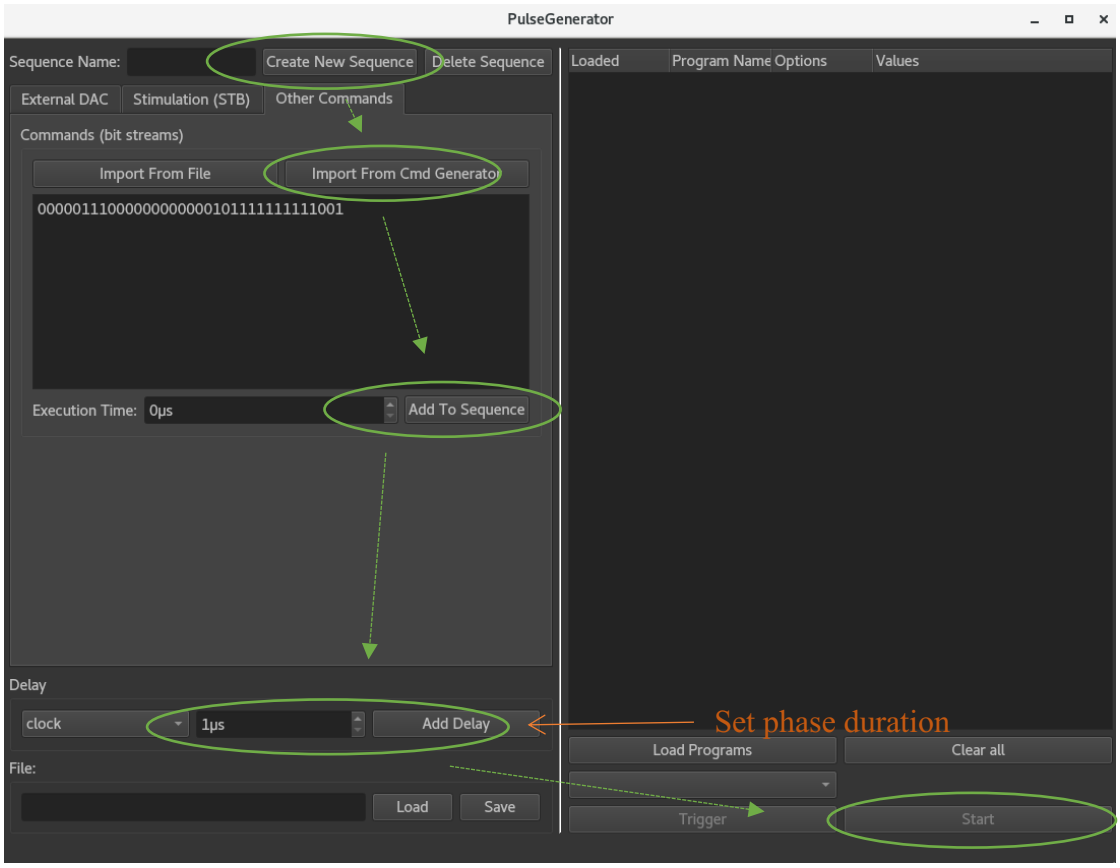

Figure A.7 Sequence creation and starting stimulation. 1) Creating a new sequence corresponding to the pulse that we want to deliver 2) Import the command generated before 3) Add the command to the sequence 4) Add the delay 5) Start stimulation.

A.3 Cross-correlation basics

In neural simultaneous recordings, a CCG is intended to compare the output between two neurons, one chosen as the reference, and the other one as the target. It is better to visualize the steps behind the calculation in order to understand the purpose of this tool.

First of all, spikes of each neuron are sorted and respective spike trains are plotted using a chart named raster plot, where every vertical bar corresponds to a spike that occurred at a specific time. The two spike trains are aligned (if we stimulate both the cells, the alignment is done with respect to the time of the stimulus release), and a window is chosen. The window is divided into a predefined number of segments, called bins, and it is centered for each spike of the reference cell. Then, looking at the target neuron, we count the number of spikes falling in each bin. In the example in Figure A.8, a window comprised of 6 bins is centered on the n-reference spike, and spikes of the target neuron are counted in each one of the bins, getting in this case [+1, +1, 0, +1, 0, 0]. The window is moved to the next spike (getting [+1, 0, 0, +2, 0, +1]) and the process is repeated until all spikes have been considered. Taking one bin, all the counts for every window are summed, and the CCG is finally obtained. The counts can be divided by the total number of spikes of the reference neurons to get a distribution of the spike transmission probability and make the comparison between different time points of the cell culture.

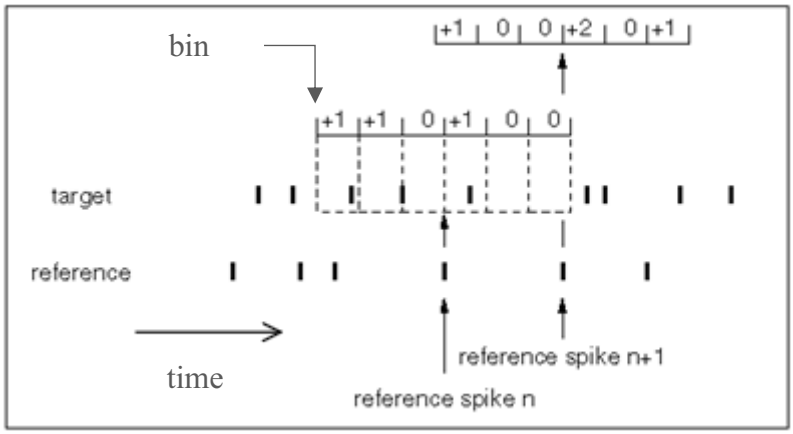

Figure A.8 Schematics of CCG calculation [57].

In a nutshell, what a CCG tells is the probability the target neurons fire around the time the reference neuron did. If there are some dependencies between the cells, this would be transferred to the CCG: generally, a flat CCG indicates no relationship, while a peak (before or after the reference spike) at a certain delay could suggest synaptic coupling (Figure A.9). Using a statistical test, we can assess the validity or not of the second option.

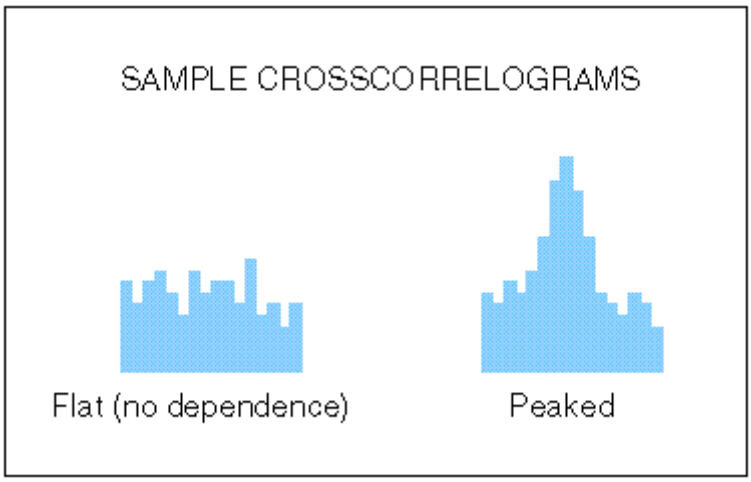

Figure A.9 A flat CCG showing no dependence, and a CCG featuring a peak implying a probable synaptic connection [57].